Wakes tbd

October 20, 2025

1 Abstract

Cold pools, formed under clouds by the evaporation of precipitation, play a central role in maintaining and organizing atmospheric convection. ~~Their~~ It is suspected thtat their absence in climate models ~~leads~~ may lead to significant errors in the representation of convection, such as the premature convection extinction after sunset. The introduction of a cold pool parameterization into the LMDZ climate model has significantly improved the representation of convection, in particular its diurnal cycle. However, this parameterization had ~~never been finely evaluated before~~ not yet been accurately evaluated in terms of ~~representation of~~ representing the cold pool properties. This work provides for the first time such an evaluation based on Large Eddy Simulation (LES). ~~We evaluate the underlying physics of the model, its internal variables as well as those used in the coupling~~ First, we evaluate the physical relationships underlying the cold pool model in the LES, then, in a second step, its behavior when coupled with the deep convection scheme ~~. The LES analyses~~ in the single-column version of LMDZ. The analyses carried out demonstrate the relevance of the assumptions ~~at the basis of~~ underlying the parameterization. ~~We also show that its initial version is able to capture~~ The initial version actually captures the main characteristics of ~~the cold pools , although some biasesare identified. These are corrected thanks to substantial modifications made~~ LES cold pools but also exhibits some biases. We show how substantial modifications to the cold ~~pools~~ pool scheme and a readjustment of ~~some free parameters . Persistent defects~~ certain free parameters helped reduce those biases significantly. The remaining flaws could be corrected by adding ~~thermal-related mixing within~~ convective mixing through thermal plumes within the cold pools and by modeling the evolution of ~~their density in a more physical way~~cold pools number density rather than imposing it.

2 Introduction

During thunderstorms, a significant amount of precipitation evaporates before reaching the ground, generating cold air masses in the layers below the clouds. This cooled air, denser than its surroundings, collapses and then spreads horizontally across the surface, forming ~~what are called~~ so-called cold pools. These are often associated with a gust front, capable of lifting the surrounding warm air and thus promoting the development of new convective cells. In organized propagative systems such as squall lines, convective columns are permanently generated by cold pool fronts at the front of the system (??). When the cold pool is accompanied by a gust front, it is called a density current. These density currents are fueled by precipitating downdrafts, which is their main dynamic driver. ~~Although present~~ Present over both continents and oceans, density currents are generally deeper, colder, and propagate more rapidly over continents. They play a key role in the self-aggregation of tropical convection (?), as well as in the transition between shallow and deep convection (??)

In atmospheric Global Circulation Models (GCMs), as those used for climate change studies, convection has to be parameterized due to the coarse horizontal resolution (30 to 300 km). Simulating convective rainfall with parameterized physics is challenging (?). GCMs often underestimate rainfall rates (???) and produce peak precipitation at noon, in phase with insolation, while the maximum precipitation is generally observed in late afternoon or during night (????). Density currents probably play a key role in this timing, by self-maintaining convection (??). One of the first attempts to parameterize density currents was proposed by ?. Later on, ? proposed a parameterization based on a population of identical circular density currents that are cooled by convective precipitation. The coupling of the ? parameterization of deep convection with this cold pool parameterization and with the thermal plume model of ? in the LMDZ climate model significantly improved the simulation of the diurnal cycle of precipitation in the tropics (?), shifting its maximum from noon to mid afternoon. A further improvement was brought by the introduction of the stochastic triggering of deep convection (?) which made the simulated convection more intermittent. Despite this success, and the use of the cold pool model in the standard version of the LMDZ atmospheric and IPSL (Institut Pierre Siméon Laplace) coupled models (??), it was not evaluated in details so far. At the same time, other parameterizations have been develop to include the impact of cold pools on convection, but without necessarily evaluating in details simulated cold pool characteristics and properties (??). This is explained not only by a lack of observational data but also by the fact that the internal variables of parameterizations are not directly accessible from observations.

Large Eddy Simulations (LES) are a useful complement to observations. Their fine horizontal resolution enables them to simulate explicitly turbulent and convective motions in the boundary layer (??). One advantage of LES compared to observations is that they provide full three-dimensional information. They have been used extensively to develop and evaluate boundary layer and convection parameterizations (????). LES have been used to simulate and understand cold pools (???), as well as to develop parameterizations of cold pools (?). However, their use for a cold pool parameterization assessment remains unexplored.

Here we propose to use LES to evaluate in details the parameterization of cold pools of LMDZ (??). We first use LES to evaluate some of the fundamental relationships between large scale state variables (for LES, the horizontal average over the domain) and internal variables which are at the basis of the parameterization. We then propose improvements which are further assessed in simulations with a Single-Column-Model (SCM) version of LMDZ against LES. In such simulations, the parameterization ~~interact~~ interacts with all the other parameterizations and depend on the values of a number of free parameters. To explore the sensitivity of the results to those free parameters and retune the model after improvement of its physical consent, we use a tool for automatic calibration, High-Tune-Explorer, developed recently (??). This tool, based on history matching, can be used to characterize the subspace of parameter values for which the model is in agreement with LES, given a series of target metrics and associated tolerance to error (?). It is used here to explore the sensitivity of the agreement between SCM simulations and LES to the model free parameters.

The paper starts by presenting in the section 1 the tools used: the LMDZ model, the cold pool parameterization by ? (referred to as the GL10 hereafter), and the LES used for evaluation. The presentation of the tuning tool (largely published) and the setup of its use is let to an appendix to concentrate on model physics and improvement in the core of the paper. In section 2, we detail the cold pool sampling in LES, designed to assess the physical laws internal to the cold pool parameterization and its coupling with deep convection. Section 3 is devoted to a comparison of cold pool model variables simulated by LMDZ in SCM mode and those calculated in LES, in order to identify the model's limitations. These results will then be discussed, and proposed improvements will be detailed in section 4. Finally, we conclude with a synthesis and discussion of prospects in section 5.

3 Tools and methods

3.1 LMDZ and its single-column version

LMDZ is the General Circulation Model (GCM) used in this work. Developed in the 1970s at ~~the~~ Laboratoire de Meteorologie Dynamique (??)~~, the~~. The "Z" in LMDZ refers to the model's ability to refine (or zoom) its horizontal grid over a specific region. This climate model is based on simplified Navier-Stokes equations for fluid mechanics, as well as transport equations. It represents the second generation (?) of a climate model initially described by Sadourny and Laval (1984). LMDZ is the atmospheric component of the IPSL coupled model. The latter is one of around twenty coupled models taking part in major international model intercomparison exercises, such as those of the CMIP (Coupled Model Intercomparison Project), the results of which are used in IPCC (Intergovernmental Panel on Climate Change) reports. We use here the LMDZ6A configuration of LMDZ designed for CMIP6 and described by ?.

LMDZ consists of two main parts, from a physical, mathematical and computational point of view. The first part, called "the dynamics", concerns the numerical resolution of the atmospheric general circulation equations. This component manages horizontal exchanges between the model's grid cells. The second part, called "physics", calculates the impact of radiation, small-scale processes (subgrid) and phase changes of water on dynamic variables via "physical parameterizations". This "physical" part is made up of juxtaposed atmospheric columns, which do not interact with each other. Within each column, the variables are assumed to be statistically homogeneous in the horizontal plane.

The SCM version of LMDZ is built by extracting an atmospheric column from the GCM, incorporating all subgrid-scale parameterizations, and running it in a large-scale constrained environment. This approach has become central in the development and tuning of parameterizations of convection and associated clouds in several climate modeling groups (**??**). Parameterizations are often developed and evaluated within this single-column framework by comparing them with LES of the same atmospheric column. The SCM/LES approach was promoted in particular by GCSS (GEWEX Cloud Systems Study), a program aimed at improving the parameterization of cloud systems in climate models (**?**). A major advantage of the SCM is its low computational cost, which allows a large number of simulations, even on a laptop, making it particularly useful in the development phase, where extensive testing is required.

3.2 Convective parameterizations in LMDZ

The role of convective parameterizations is to provide sources of heating Q_1 and moistening Q_2 to the conservation equations of potential temperature θ en specific humidity qv :

$$C_p \frac{D\theta}{Dt} = Q_R + (L_v + f_g L_f)(c - e) - C_p \frac{1}{\rho} \frac{\partial \rho \overline{w'\theta'}}{\partial z} \quad = \quad Q_R + Q_1 \tag{1}$$

$$\frac{Dqv}{Dt} = e - c - \frac{1}{\rho} \frac{\partial \rho \overline{w'qv'}}{\partial z} \quad = \quad -Q_2/L_v \tag{2}$$

where C_p is the heat capacity of dry air, Q_R is the radiative heating, c and e are condensation and evaporation rates, f_g is the condensate ice fraction, L_v is the latent heat of vaporization and L_f the latent heat of fusion. For any state variable ϕ, the source term should include the vertical convergence of the Reynolds turbulent flux of the quantity $-\partial_z \rho \overline{w'\phi'}/\rho$, representing the effect of subgrid-scale turbulent or convective motions on the explicitly resolved large scale flow. The convective parameterizations also often provide a source term Q_3 for momentum but it is not involved in the coupling with cold pools described here.

Note that the equations above are simplified assuming that the ice fraction f_g is unchanged by evaporation and condensation. Note also that Q_2 is a sink of humidity expressed conventionally as a heating term with constant L_v.

The parameterization of turbulence, convection and clouds in LMDZ is based on a multi-scale, or object view. ~~The small scale turbulence,~~

The small scale turbulence, mainly active near the surface, is accounted for following **?** scheme, with an eddy diffusive approach in which the eddy diffusivity relies on a prognostic equation for the turbulent kinetic energy. ~~A specific mass flux parameterization, the thermal plume model, accounts~~

The thermal plume model was developed specifically to account for the vertical transport by organised thermal ~~plume~~plumes, cells or rolls in the convective boundary layer (**??**). ~~It was later on coupled to a bigaussian statistical representation of the subgrid distribution of humidity, leading~~ The population of convective structures within a grid cell are summarized into a mean ascending plume, with a unique mass ascending mass flux $f_{th} = \rho \alpha_{th} w_{th}$, compensated by a mass flux $-f_{th}$ in a fraction $1 - \alpha_{th}$ of the grid cell. The sources $Q_1{}^{\text{th}}$ and $Q_2{}^{\text{th}}$ only contain the vertical convergence of the mass flux transport ($\rho \overline{w'\phi'} = f_{th}(\phi_{th} - \phi)$ where ϕ_{th} is the value of variable ϕ within the thermal plume), the part coming from the condensation or evaporation being treated in the so-called large-scale condensation scheme.

The large-scale condensation scheme is used to predict the cloud fraction except for deep convection, based on a probability distribution function (PDF) of the total water within the horizontal grid cell (giving the cloud fraction as the part of the grid cell with humidity above saturation). This statistical cloud scheme provides to first order: $Q_1{}^{\text{lsc}} = (L_v + f_g L_f)(c - e)$ and $Q_2{}^{\text{lsc}} = -L_v(c - e)$. For shallow cumulus or strato-cumulus, cloud condensation is thus treated outside the thermal plume scheme. Both schemes are however coupled together when the thermal plume is active within a grid cell. In this case, the subgrid water PDF is prescribed as a bimodal function, with one mode corresponding to the thermal plume and the other one to its environment. This coupling led to a strong improvement in the representation of cumulus and stratocumulus clouds (**??**). ~~Deep convection~~

Deep convection is represented with a modified version of the **?** scheme. ~~.~~ As for shallow convection, the parameterization of deep convection represents a population of cumulonimbus clouds that would occur in the grid cell as an effective cumulonimbus cloud. However, for deep convection, the transport, condensation, cloud formation and rainfall are treated within the same scheme.

Convective transport in these cumulonimbus clouds is represented by mass fluxes and an air exchange matrix. Several "compartments" can be distinguished. **An undiluted updraft** that does not entrain air laterally above the base of the cloud, but is gradually "peeled" or "eroded" while rising. It is assumed to be fast enough to carry with it the liquid or solid water condensed within it. **A population of diluted ascending or descending air masses, saturated,** created by mixing a fraction of air peeled from the adiabatic ascent with ambient air according to an imposed PDF. It is divided into bins defining a population of air parcels that are "sent" to their neutral buoyancy level (layer), thus creating a matrix in which each term is an exchange of air between two layers of the model. Before forming these mixtures, the water in excess in the air peeled from the adiabatic updraft is precipitated, and then again, the excess water is precipitated before the diluted updraft or downdraft is detrained into the environment. Finally **the unsaturated downdrafts** receive all the rain formed during peeling or detraining in the environment. Some of these descents take place outside the clouds, in air that is not saturated with moisture, allowing them to evaporate. This evaporation of very large quantities of rain forces strong downdrafts. Below the base of the clouds, all of the precipitation is outside the clouds. Their re-evaporation is the source of density currents, or cold pools, created under cumulonimbus clouds.

In practice, the convective tendencies Q_1 and Q_2 are separated into two parts, "saturated" and "unsaturated". The saturated tendencies ${Q_1}^{\rm sat}$ and ${Q_2}^{\rm sat}$ take into account adiabatic updraft, diluted updrafts and downdrafts, and a downward flux in the environment compensating all these mass fluxes. The unsaturated tendencies ${Q_1}^{\rm unsat}$ and ${Q_2}^{\rm unsat}$ take into account unsaturated downdraft as well as compensatory ascent.

The main modification of the deep convection scheme concerns the mixing formulation (?) and the triggering and closure formulations (**??**) modified so that deep convection is controlled by sub-cloud processes: boundary-layer thermals (?) and cold pools (?). The cold pool scheme and the control of convection by sub-cloud processes, particularly the role of cold pools, will be detailed in the following sections.

3.3 The cold pool model

The cold pool model represents a population of identical circular cold pools (~~the~~ or wakes) over an infinite plane containing the grid cell. All the wakes have the same height, radius, and vertical profiles of thermodynamic variables. Their centers are statistically distributed with a uniform density $\cancel{D_{wk}}D_{\rm wk}$. Cold pools divide the space into two parts: (i) the interior of cold pools (w) is where convective precipitating downdrafts fall; in these downdrafts, the re- evaporation of precipitation generates intense cooling and strong negative buoyancy; (ii) the exterior of cold pools (x) contains the warm air that fuels the saturated convective currents (Fig. 1). The top height of the cold pool ~~(h_{wk})~~ is defined as the altitude $h_{\rm wk}$ (and associated pressure $p_{\rm wk}$) where the temperature difference between (w) and (x) becomes zero. Below this level cold pools are cooler than their exterior: they collapse and spread out as they are denser than the surrounding air. The boundary between the cold pool and the environment is considered to be infinitely thin, and at each point on this boundary, the cold pool spreads at a rate C. C is considered to be a random variable whose mean C_* will give the rate at which the cold pool spreads. In the GL10 model, C_* scales with the square root of the potential energy available in the cold pools, i.e the cold pool's collapse energy, $WAPE$ (Wake Available Potential Energy), given by:

$$WAPE = g\int \frac{\delta\rho}{\overline{\rho}} = -g\int_0^{\cancel{h_{wk}}\,h_{\rm wk}} \frac{\delta\theta_v}{\overline{\theta_v}}dz \qquad (3)$$

so that:

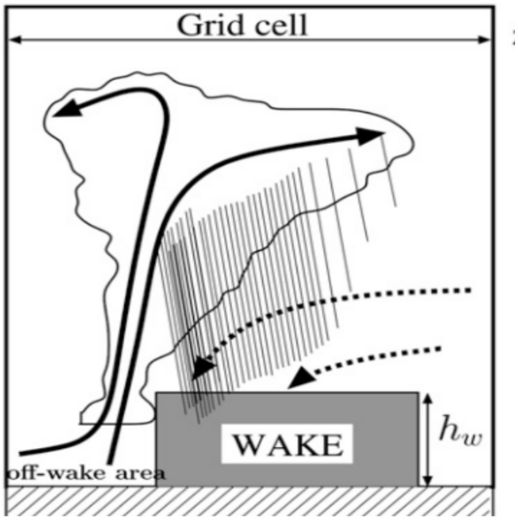

Figure 1: Conceptual diagram of a density current (?).

$$C_* = k\sqrt{2WAPE} \tag{4}$$

where ρ is the air density; θ_v is the virtual potential temperature.

For any variable X, $\delta X = X_w - X_x$ is the difference of its mean value in the two subdomain and $\overline{X}$ the average over the horizontal domain.

~~So far,~~ Coefficient k in equation (4) ~~is fixed, to~~ should take a value between 0 and 1. This coefficient should probably depend on the structure of cold pools. Based on 3D CRM (Cloud Resolving Models) simulations, Lafore (2000) estimated this coefficient at 0.33 in the case of a linear structure such as squall grain. This is the value ~~used in the GL10 model~~retained in LMDZ6A.

The spread rate of cold pools C_* is deduced from the following relationship:

$$\partial_t \sigma_{wk} = 2\pi r C_* \underline{D_{wk}} D_{\mathrm{wk}} = 2C_* \underline{\sqrt{\pi D_{wk}\sigma_{wk}}}\sqrt{\pi D_{\mathrm{wk}}\sigma_{wk}} \tag{5}$$

where σ_{wk} is the surface fraction covered by cold pools ($\sigma_{wk} = \cancel{D_{wk}\pi r^2} D_{\mathrm{wk}}\pi r^2$). Due to the complex life cycle of cold pools (including birth, death, collisions and mergers), calculating their number density requires an other parameterization. ~~In this study, as in GL10 model~~So far, the value of the cold pool number density is thus imposed. In ~~GL10 model~~LMDZ6A, this density is fixed to a different value over ocean (~~$10.10^{-10}\ m^{-2}$, i.e.~~ 10 cold pools over 100 km×100 km) and over the continent (~~$8.10^{-12}\ m^{-2}$, i.e. around~~ 8 cold pools over 1000 km×1000 km). In the GL10 model, cold pools initially appear with a surface fraction of 2% and evolve over time according to equation 5. The evolution of σ_{wk} is arbitrarily limited to a maximum of 40% ($\sigma_{wk} \leq 0.4$).

Those thresholds are one limitation of the scheme that we hope to remove in the future.

It is assumed that below the top of cold pool ($\cancel{h_{wk}}p_{\text{wk}}$), the vertical velocity profile associated with the subsidence of the cold pool results solely from the spreading at the surface, without lateral entrainment (e_w) or detrainment (d_w) between the cold pool and its environment. Above this level, the subsidence ~~is driven both by the need to fed the subsidence in~~ induces a lateral convergence of air feeding the cold pool ~~(air mass continuity equation) and by the~~ which can be reinforced by additional reevaporation of rainfall below stratiform clouds. The shape of the vertical profile of the velocity difference $\delta\omega$ between the cold pool region and its environment is imposed as a piecewise linear function of pressure: $\delta\omega$ increases linearly from zero at the surface up to a maximum value at $\cancel{h_{wk}}$ p_{wk} and then decreases linearly between ~~h_{wk} and a maximum height at which it cancels : h_m~~ p_{wk} and a minimum pressure p_{upper} corresponding to the upper bound of the cold pool model. The vertical subsidence which thus increases downward between ~~h_m and h_{wk}~~ p_{upper} and p_{wk} is fed by lateral entrainment ~~$(e_w > 0)$~~

$$e_w = \sigma_{wk}(1 - \sigma_{wk})\partial_p\delta\omega + \partial_t\sigma_{wk} \tag{6}$$

without detrainment.

This lateral entrainment accounts for the horizontal component of the meso-scale circulation known to entrain air from low- or mid- tropospheric air into the cold pool.

At $\cancel{h_m}p_{\text{upper}}$, the top of the cold pool model, δ_X ~~,~~ cancels for all cold pool state variables.

In GL10 model ~~, h_m~~ and in LMDZ6A, p_{upper} was set to 600 hPa and there was also a nonzero velocity difference ($\delta\omega^{cv}$) at $\cancel{h_m}p_{\text{upper}}$, accounting for the difference of the convective mass fluxes between (w) and (x). In the version used in this paper, this difference is now zero ($\delta\omega^{cv} = 0$) above this level.

~~The evolution of the potential temperature difference ($\delta\theta$) between (w) and (x) is controlled by differential heating (δQ_1^{cv}, δQ_1^{wk}) due to deep convection and~~ It is the re-evaporation of rain in unsaturated downdrafts that is the primary driver of cold pools development. This process is reflected in the model by assigning the heating term ${Q_1}^{\text{unsat}}$ to the interior of cold pools, ~~as well as by damping due to gravity waves (τ_{gw}). The humidity difference (δq) follows a similar pattern, but without the damping effect of gravity waves. Heat sources are replaced by moisture sources (δQ_2^{cv} for convection and δQ_2^{wk} for cold pools).~~

while ${Q_1}^{\text{sat}}$ acts on their environment. Consistent with this splitting, we assume that the saturated part of the convective scheme sees the profiles outside the cold pools, and the unsaturated downdrafts their interior. We further assume that thermal plumes are only active in the fraction of the horizontal surface located outside the cold pools. The thermal plume model therefore induces a differential tendency that is opposite of the average tendency. Ultimately, the contrast in convective tendencies (shallow and deep) between the cold pools and their environment reads:

$$\begin{cases} \delta {Q_1}^{\text{cv}} = \frac{{Q_1}^{\text{unsat}}}{\sigma_{wk}} - \frac{{Q_1}^{\text{sat}}}{1-\sigma_{wk}} - {Q_1}^{\text{th}} \\ \\ \delta {Q_2}^{\text{cv}} = \frac{{Q_2}^{\text{unsat}}}{\sigma_{wk}} - \frac{{Q_2}^{\text{sat}}}{1-\sigma_{wk}} - {Q_2}^{\text{th}} \end{cases} \tag{7}$$

~~where L_v is the latent heat of vaporization of water and~~ It is the terms $\delta Q_1{}^{\rm cv}$ and $\delta Q_2{}^{\rm cv}$ that drive the time evolution of $\delta\theta$ and δq given by:

$$\cancel{\tau_{gw} = \frac{\sqrt{\sqrt{\sigma_{wk}} - (1-\sqrt{\sigma_{wk}})}}{4Nz\sqrt{D_{wk}}}} \begin{cases} \partial_t \delta\theta = \frac{\delta Q_1{}^{\rm cv} + \delta Q_1{}^{\rm wk}}{C_p} - \overline{\omega}\partial_p\delta\theta - \frac{K_{gw}}{\tau_{gw}}\delta\theta, \\ \partial_t \delta q = \frac{\delta Q_2{}^{\rm cv} + \delta Q_2{}^{\rm wk}}{L_v}. - \overline{\omega}\partial_p\delta q \end{cases} \tag{8}$$

~~is estimated as the time required for a wave with speed Nz to travel a distance equal to the geometric mean of the cold pool size and the interval between cold pools. C_p is the heat capacity of dry air , N is the Brunt-Väisälä frequency, and z is altitude. K_{gw} is an efficiency of gravity waves.~~

~~δQ_1^{wk} (respectively δQ_2^{wk}) depend on the entrainment (e_w) of dry air, the differential advection of $\overline{\theta}$ (respectively $\overline{q}$) and $\delta\theta$ (respectively δq):~~

$$\cancel{\begin{cases} \frac{\delta Q_1^{wk}}{C_p} = \frac{e_w}{\sigma_{wk}}\delta\theta - \delta\omega\partial_p\overline{\theta} - (1-2\sigma_{wk})\delta\omega\partial_p\delta\theta \\ \frac{\delta Q_2^{wk}}{L_v} = \frac{e_w}{\sigma_{wk}}\delta q - \delta\omega\partial_p\overline{q} - (1-2\sigma_{wk})\delta\omega\partial_p\delta q \end{cases}}$$

This time evolutions also includes a differential heating and moistening by the cold pools itself of the air inside and outside the cold pools, under the effect of lateral air entrainment from the environment above $p_{\rm wk}$, subsidence inside the cold pools, and compensatory ascendance in the environment:

$$\begin{cases} \frac{\delta Q_1{}^{\rm wk}}{C_p} = -\frac{e_w}{\sigma_{wk}}\delta\theta - \delta\omega\partial_p\overline{\theta} - (1-2\sigma_{wk})\delta\omega\partial_p\delta\theta \\ -\frac{\delta Q_2{}^{\rm wk}}{L_v} = -\frac{e_w}{\sigma_{wk}}\delta q - \delta\omega\partial_p\overline{q} - (1-2\sigma_{wk})\delta\omega\partial_p\delta q \end{cases} \tag{9}$$

~~Similarly, δQ_1^{cv} (respectively δQ_2^{cv}) are computed from the by heating tendencies associated with unsaturated currents ($Q_{cv}^{1,unsat}$, or $Q_{cv}^{2,unsat}$ for humidity) and saturated currents ($Q_{cv}^{1,sat}$, or $Q_{cv}^{2,sat}$ for humidity):~~ The terms $-\overline{\omega}\partial_p\delta$ in (8) partially compensate for the fact that the contrasts δ are not transported by the dynamics until now. We therefore take into account, in the parameterizations, the vertical part of large-scale advection to partially compensate for this deficiency.

Finally, the last term, present only in the θ part of (8), corresponds to the reduction in temperature contrasts by gravity waves with a coefficient specified as the ratio of an efficiency K_{gw} to a time constant

$$\tau_{gw} = \frac{\sqrt{\sqrt{\sigma_{wk}} - (1-\sqrt{\sigma_{wk}})}}{4Nz\sqrt{D_{\rm wk}}} \tag{10}$$

~~$Q_{cv}^{x,unsat}$ and $Q_{cv}^{x,sat}$ ($x = 1, 2$) are given by the deep convection scheme as described in ?.~~

~~Entrainment is determined from the vertical gradient of $\delta\omega$ and~~ estimated as the time required for a wave with speed Nz (where N is the Brunt-Väisälä frequency and z is altitude) to travel a distance equal to the geometric mean of the cold pool ~~spreading rate, according to the following relationship:~~

$$\cancel{e_w = \sigma_{wk}(1 - \sigma_{wk})\partial_p \delta\omega + \partial_t \sigma_{wk}}$$

~~Equation ??, via the variables δQ_1^{cv} and δQ_2^{cv}, describes the impact of deep convection on cold pools which results in their cooling due to precipitating descents, as discussed above.~~ size and the interval between cold pools

The cold pool model is now fully described. It includes:

- three prognostic variables, derived directly from the model equations: the profiles of $\delta\theta$ and δq and σ_{wk}.
- three diagnostic variables, evaluated from the profile of $\delta\theta$: ~~h_{wk}~~p_{wk}, C_* and $WAPE$
- three main free parameters: the coefficient k, the density ~~D_{wk}~~ D_{wk} and τ_{gw}.

3.4 ~~Coupling with~~ Triggering and closure of the deep convection ~~model~~scheme

In LMDZ, deep convection is triggered when the Available Lifting Energy (ALE) at cloud base exceeds the convective inhibition (CIN) threshold. This can be caused either by uplift energy from the convective boundary layer (~~ALE_{bl}~~ALE_{bl}), provided by the thermals model (?), or by energy generated by cold pools (~~ALE_{wk}):~~ ALE_{wk}):

$$\max(\cancel{ALE_{bl}}ALE_{\mathrm{bl}}, \cancel{ALE_{wk}}ALE_{\mathrm{wk}}) > |CIN| \tag{11}$$

The intensity of the convection depends on the mass flux (M_b) at the cloud base, determined from the availbale lifting power ALP, provided by thermals (~~ALP_{bl}~~ALP_{bl}) and cold pools (~~ALP_{wk}~~ALP_{wk}).

$$M_b = k \cancel{\frac{ALP_{bl} + ALP_{wk}}{(2w_b^2 + |CIN|)}} \frac{ALP_{\mathrm{bl}} + ALP_{\mathrm{wk}}}{(2W_b^2 + |CIN|)} \tag{12}$$

~~where k and w_b (~~where

$$W_b = wb_{\mathrm{srf}} + \frac{wb_{\mathrm{max}}}{1 + \frac{\Delta P}{(P_s - P_{LFC})}} \tag{13}$$

is the vertical velocity at the level of free convection ~~) are~~ (LFC), $\Delta P = 500$ hPa and k, wb_{srf} and wb_{max} are model free parameters.

~~Regarding thermal triggering, a~~ Concerning the boundary layer, the available lifting energy is taken as the maximum kinetic energy in the thermal plume below cloud base

$$ALE_{\mathrm{bl}} = \frac{1}{2} {w_{th,max}}^2 \tag{14}$$

A notable improvement was introduced by ?, with the implementation of a statistical representation of the size distribution of cloudy thermal bases. ~~The triggeringof deep convection by thermals occurs when~~ In the new statistical triggering, deep convection is activated if both $ALE_{th} > |CIN|$ and at least one cumulus cloud within a grid cell exceeds a given size, specified by S_{trig} (adjustable parameter).

~~The two variables ALE_{wk} and ALP_{wk} have been introduced by ? to take account of the effect of cold pools on convection~~The available lifting power scales with ${w_{th,max}}^3$.

~~To calculate ALE_{wk}~~

To calculate ALE_{wk}, the model assumes that the maximum speed (C_{max}) on the cold pool contour will trigger convection. This is assumed to be proportional to the square root of $WAPE$, with a higher coefficient of proportionality than the one used for C_* leading to the following relationship:

$$C_{\mathrm{max}} = k' \sqrt{2WAPE} \tag{15}$$

where k'=~~1~~
1.

The Available Lifting Energy associated with cold pools is thus expressed by the following relationship:

$$ALE_{wk} ALE_{\mathrm{wk}} = \frac{1}{2} C^2_{\mathrm{max}} \tag{16}$$

Combining equations (16) and (15)~~gives the expression for ALE_{wk} below:~~
, one obtains:

$$ALE_{wk} ALE_{\mathrm{wk}} = k'^2 WAPE \tag{17}$$

With $k' = 1$, this equation says that, in the cold pool model, the Available Lifting Energy associated with cold pools is equal to the collapse energy.

~~ALP_{wk}~~ ALP_{wk} is calculated assuming that cold pools exert a horizontal power on the surrounding air during its spreading. This horizontal power is then converted into vertical power. During this conversion, the model assumes that a large part of the horizontal power is dissipated, and that only 25% contributes to increasing the intensity of convection.

Each cold pool generates its own lifting power, depending on its spreading speed (C_*), height (~~h_{wk}~~h_{wk}) and the length (L_g) of its gust front. The total power (~~ALP_{wk}~~ALP_{wk}) of the cold pools is the product of the power supplied by each pool times the cold pool number density (~~D_{wk}~~D_{wk}).

$$ALP_{wk} ALP_{\mathrm{wk}} = \epsilon \frac{1}{2} \rho C^3_* h_{\mathrm{wk}} L_g D_{wk} D_{\mathrm{wk}} \tag{18}$$

where $\epsilon = 0.25$ is the lifting efficiency with

$$L_g = 2\pi r \tag{19}$$

$$\sigma_{wk} = \underline{D_{wk}} D_{\text{wk}} \pi r^2 \tag{20}$$

Then, the lifting power ~~ALP_{wk} reads:~~
ALP_{wk} reads:

$$\underline{ALP_{wk}} ALP_{\text{wk}} = \epsilon \rho C_*{}^3 \underline{\sqrt{\sigma_{wk} D_{wk} \pi}} h_{\text{wk}} \sqrt{\sigma_{wk} D_{\text{wk}} \pi} \tag{21}$$

3.5 Large Eddy Simulations

Atmospheric Large Eddy Simulations (LES) are ~~numerical tools for simulating atmospheric phenomena with a horizontal resolution of tens to hundreds of meters. They are particularly well suited to the study of the thermodynamic structure of the boundary layer, as they resolve the eddies that form there. They offer an explicit and detailed representation of turbulent and convective movements within the boundary layer and associated clouds (??) .~~ performed with non hydrostatic models, with a grid resolution fine enough to resolve the main structures (large eddies) that dominate the turbulent or convective transport. They have been widely used to study the convective boundary layer with grid resolutions of a few tens of meters (??). In the presence of water phase changes, however, these simulations can become more dependent on the microphysical schemes used. One of the major strengths of LES lies in its ability to provide three-dimensional information not available from observations, making them an indispensable complement to the latter for understanding processes. In addition, LES can be used to validate the internal variables of parameterizations, enabling their physical realism to be assessed.

In this study, we use the outputs of two oceanic LES and one continental LES.

Both oceanic LES were carried out in Radiative-Convective Equilibrium (RCE) mode. RCE is a concept in which equilibrium is achieved between convective heating and radiative cooling of the atmosphere. A detailed description of RCE simulation protocols is provided in ?. In the RCE simulations used here, radiative computation is replaced by a constant cooling of -1.5 K per day, while the surface temperature is imposed. The destabilization leads to convection. The associated heating rate, largely corresponding to the release of latent heat by cloud condensation in convective towers, compensates for the cooling once quasi-equilibrium has been reached. Two oceanic LES of this RCE are used here, one is performed with the SAM model (?) and the other one with MesoNH (?). Both simulations cover an oceanic domain of 200 km×200 km with horizontal resolution of 250 m. The lateral boundary conditions are cyclic for both models. The sea surface temperature is set at 300 K. These two RCE simulations run for 44 days, with quasi steady-state regime reached after about 40 days. Output are available every 3 hours for SAM and every 24 hours for MesoNH.

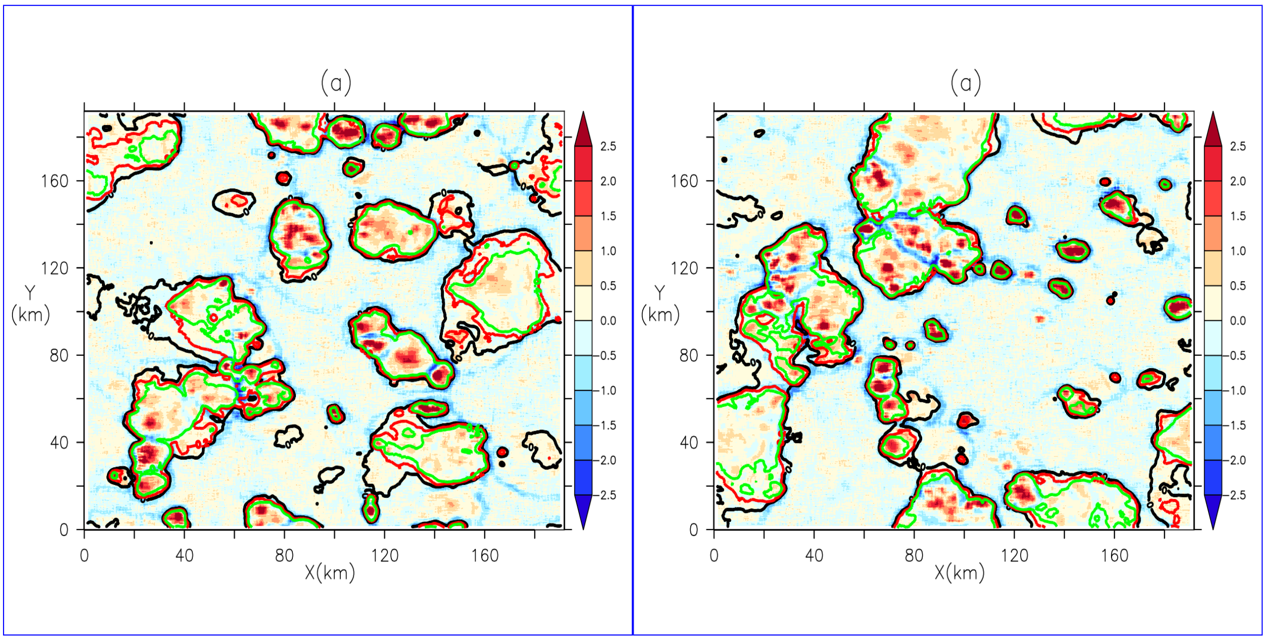

Figure 2: Moving average (with a box of 3.25 km $\times$ 3.25 km) of the divergence of wind at 10 m (in unit $10^{-3}s^{-1}$ or 1 m/s/km). Panels a and b correspond to two different states of the LES SAM carried out on the oceanic RCE case. Contours of temperature anomalies at 10 m at -0.4 K (green), -0.2 K (red) and 0 K (black) are superimposed on the smoothed divergence field.

The continental LES is based on the AMMA (African Monsoon Multidisciplinary Analysis) case. This case is derived from observations made on July 10, 2006 during the AMMA field campaign (?), during which a relatively small, short-lived convective system formed over Niamey (?). This system, with a lifetime of around 6 hours, was observed by various instruments (radar and atmospheric soundings), supplemented by satellite data. This case study represents a typical example of deep convection in the Sahel regions (?). LES for this continental case is carried out with the MesoNH model over a 200 km $\times$ 200 km domain, with a horizontal resolution of 200 m. Lateral boundary conditions are cyclic and surface fluxes are imposed. Outputs are generated at a frequency of 30 minutes.

4 Assessment of the cold pool model internal equations from LES

4.1 Distinguishing the cold ~~pool region~~ pools from ~~its~~ their environment

In order to use LES for the assessment of the cold pool parameterization, the first challenge is to separate cold pools from their environment. Indeed, there is no a priori established

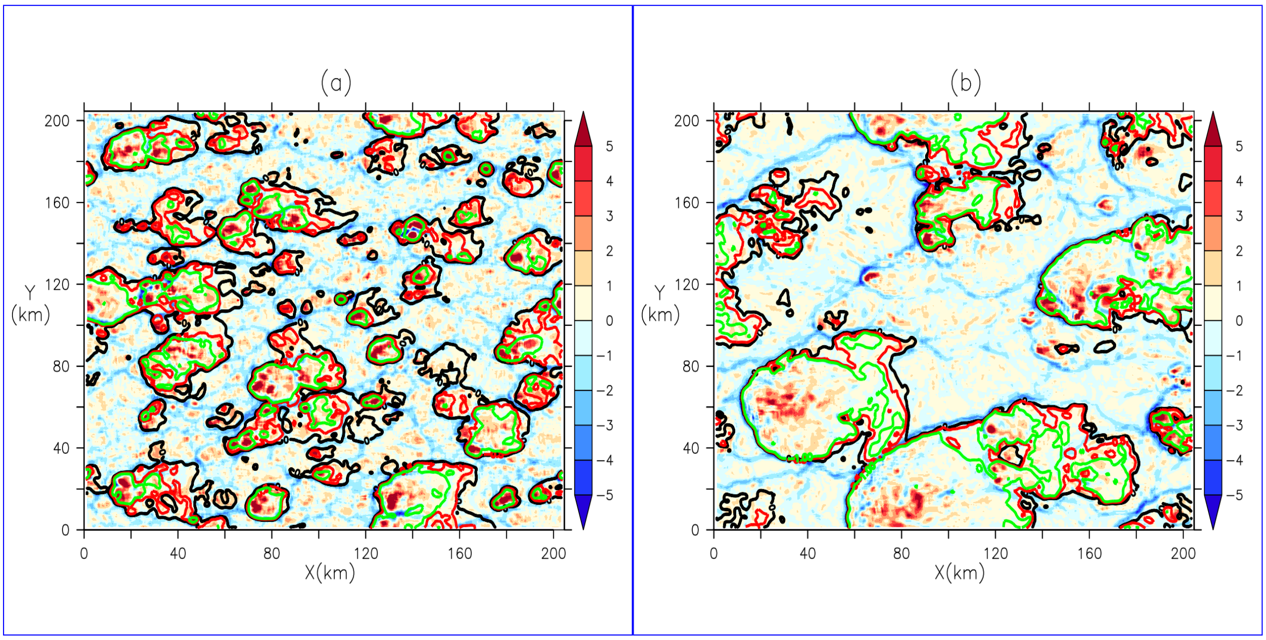

Figure 3: Same as Fig. 2 for two successive instants, 5:30 PM (a) and 7:30 PM (b), of the LES MESONH carried out on the AMMA case. The contours superimposed corresponds to $T_{10\mathrm{m}}$ anomalies of -1 K (green), -0.5 K (red) and 0 K (black).

framework for objectively identifying cold pools in observations and numerical models (**?**), and choices may depend in part on the physical picture one has of cold pools, and also, for the purpose at hand, on the picture underlying the parameterization. The first method for identifying cold pools proposed by **?** was based on surface precipitation rates. In more recent studies, such as those by **?????**, the detection of cold pools is closer to a density current oriented detection, in which variations in temperature, pressure and wind are taken into account.

In the present study, the aim is not to isolate individual “cold pools objects”, but only to know whether a grid ~~box~~ cell of the LES is inside or outside ~~a cold pool~~cold pools. Also the boundary conditions are idealized targeting the statistical homogeneity assumption that is at the basis of the Reynolds decomposition between dynamical core and physics parameterizations. In this idealized case with uniform surface temperature, cold pools can be identified fairly immediately using a threshold on the anomaly (after removing the domain average) of temperature at 10 m above surface, $T_{10\mathrm{m}}$, i.e. at the first model mid layer.

~~and~~ Fig. 2 and 3 show a horizontal ~~sliding~~ moving average with a box of 3.25 km×3.25 km of the divergence of the wind at 10 m above surface, $\overrightarrow{V_{10\mathrm{m}}}$. From these maps, the centers and gust fronts of cold pools can be easily identified, corresponding respectively to the maximum and minimum of divergence values. Maxima of divergence of surface wind indicate the center of cold pools where cold air masses collapse. Precipitation is generally co-located with these divergence maxima (not shown). The fairly strong wind convergence observed around cold pools centers corresponds to the strong lift of air masses created upstream of the gust front at the cold pool's periphery.

~~Sliding average (with a box of 3.25 km × 3.25 km) of the divergence of wind at 10 m $\overrightarrow{V_{10\text{m}}}$ (in $10^{-3}s^{-1}$). With this unit, a value of 1 corresponds to a change of wind intensity of 1 ms^{-1} for 1 km). Panels a and b correspond to two different states of the LES SAM carried out on the oceanic RCE case. Contours of temperature anomalies at 10 m at -0.4 K (green), -0.2 K (red) and 0 K (black) are superimposed on the smoothed divergence field.~~

~~Same as for two successive instants, 5:30 PM (a) and 7:30 PM (b), of the LES MESONH carried out on the AMMA case. The contours superimposed corresponds to $T_{10\text{m}}$ anomalies of -1 K (green), -0.5 K (red) and 0 K (black).~~

Both the two LES of the RCE case and the LES of the AMMA case show cold pools ~~groupings (clusters)~~ clusters forming a common gust front. This can be explained by the fact that, during propagation, cold pools can merge to create a single, larger cold pool. We can also observe that wind convergence ~~is generally more intense between the centers of grouped cold pools, indicating that updrafts of air masses associated with gust fronts is more pronounced when these~~ (and thus associated updrafts) is more intense where cold pools meet. This is in line with some studies that indicate that convection initiation on gust fronts is more efficient when two or more cold pools collide (**????**).

We superimpose on this map the $T_{10\text{m}}$ anomaly contours with different values to determine an optimal threshold for this anomaly. In the RCE case, the ~~$Tnearsrf$~~ $T_{10\text{m}}$ anomaly at 0 K sometimes includes regions without cold pools centers, where divergence of surface wind is low (~~a and~~ Fig. 2a and b) while anomaly contours at -0.2 K and -0.4 K surround the centers of cold pools quite well. In the AMMA case, figure ~~??~~3a clearly shows that the 0 K threshold is too high to identify cold pools. ~~Figure ??~~Fig. 3b, on the other hand, shows that the -1 K threshold follows gust fronts of cold pools better than the -0.5 K threshold. On the basis of these analyses, we retain the $T_{10\text{m}}$ anomaly thresholds at -0.2 K and -1 K to identify cold pools in the RCE and AMMA cases respectively.

4.2 ~~Computing cold pool anomalies vertical profiles~~

4.2 Computing the WAPE from the cold pool anomalies

Once the threshold value is fixed for the $T_{10\text{m}}$ anomaly, we separate the full 3-dimensional LES domain between cold pool region (wk) and the rest of the domain (x) form which we can compute the horizontal averages on each subdomain, X_{wk} inside cold pools and X_{x} outside, and then the cold pool anomaly $\delta X = X_{\text{wk}} - X_{\text{x}}$. This sampling allows to compute the vertical profiles of cold pools anomaly for temperature (δT), humidity (δq) and vertical velocity (δw). Examples of temperature anomalies are shown in Fig. 4.

Note that we apply the same surface mask to the entire column to determine the vertical profiles. This simple vision of vertical cylinders is adopted to match the view underlying the parameterization but may be put into question in the presence of ~~strong~~ strongly tilted convection.

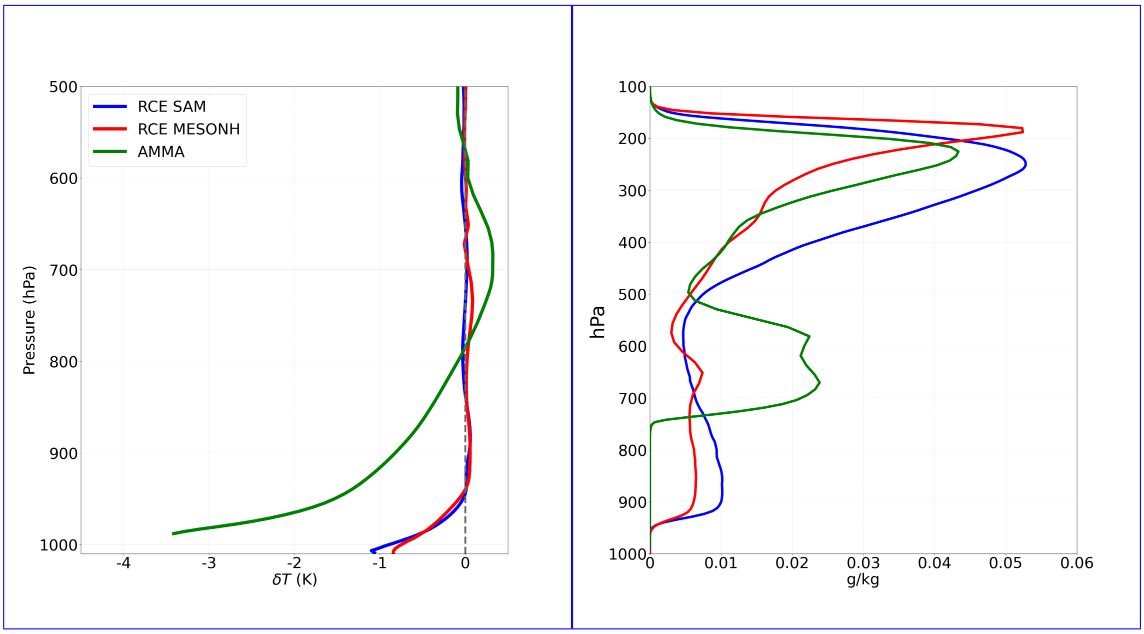

Figure 4: Vertical profiles of the cold pool temperature anomaly (left, difference between the inside and the outside of cold pools~~calculated at an instant of the LES (SAM and MESONH~~) ~~of the RCE case~~ and ~~at 7:30 PM~~ of the ~~LES for the AMMA case~~averaged condensed water (right, g/kg).

One can then compute the collapse energy ($WAPE$) of cold pools in the LES by integrating from the surface up to p_{wk}, the virtual temperature anomaly, $\delta\theta_v$ (equation, 3). As suggested by **?**, we take for p_{wk} the pressure where the δT profile cancels out. This altitude is around 950 hPa (approximately 600 m) in the oceanic RCE case and around 800 hPa (approximately 2 km) in the AMMA case (Fig. 4).

4.3 Computing ~~the spreading speed,~~ C_* ~~,~~ from ~~sampled~~ the mean wind divergence inside cold pools

It is assumed in the parameterization that cold pools are identical disks of radius r. This assumption makes it easy to determine C_* by the divergence theorem.

$$\int\int \text{div}\left(\overrightarrow{V10\text{m}}\right) dS_{wk} = C_* L_g \tag{22}$$

$$C_* = \frac{\overline{\text{div}\left(\overrightarrow{V10\text{m}}\right) S_{wk}}}{L_g} \tag{23}$$

where S_{wk} is the surface of cold pools

$$S_{wk} = \pi r^2 \tag{24}$$

Equations 19, 20 and 24 allow us to express C_* as a function of the mean divergence of wind at 10 m, the surface fraction (σ_{wk}) and the density (~~D_{wk}~~D_{wk}) of cold pools by the relation:

$$C_* = \frac{1}{2}\overline{\mathrm{div}\left(\overrightarrow{V_{10\mathrm{m}}}\right)}\,\cancel{\sqrt{\frac{\sigma_{wk}}{D_{wk}\pi}}}\sqrt{\frac{\sigma_{wk}}{D_{\mathrm{wk}}\pi}} \quad (25)$$

To apply this calculation of C_* in the LES, we take the horizontal average of the surface wind divergence inside cold pools. The surface fraction (σ_{wk}) of cold pools calculated in the LES is 0.214 (Average over the available time steps between 5:00 PM and 10:00 PM) for the AMMA case and 0.253 (Average over the 24 time steps with the SAM model) for the RCE case. To determine ~~D_{wk}~~D_{wk}, we manually counted the centers of cold pools visible on the surface wind divergence maps (~~Fig. ?? and ??~~Fig. 2 and 3), as we did not use automated detection methods in this study that could generate their number automatically. We find a density, ~~D_{wk}~~D_{wk}, of about 5 cold pools per 100 km $\times$ 100 km in the RCE case, and about 2.5 cold pools over the same domain in the AMMA case.

4.4 ~~Computing the collapse energy, WAPE, from the virtual temperature anomaly~~

~~We finally calculate the collapse energy ($WAPE$) of cold pools in the LES using equation (3) proposed by ?. The task consists of determining $\overline{\theta_v}$, as well as the profile of $\delta\theta_v$ and h_{wk} in the LES. To do this, we first computed δT in the LES, then derived $\overline{\theta_v}$ and the profile of $\delta\theta_v$. Regarding the determination of h_{wk}, as suggested by ?, we take this height at the altitude where the δT profile cancels out. This altitude is around 950 hPa (approximately 600 m) in the oceanic RCE case and around 800 hPa (approximately 2 km) in the AMMA case ().~~

4.4 Computing ALP and ALE form gust front vertical velocities

~~Here~~ Finally we derive a direct estimation of the Available Lifting Energy (~~ALE_{wk}~~ALE_{wk}) and Power (~~ALP_{wk}~~ALP_{wk}) in the LES from a sampling of the vertical wind at cloud base.

To do this, we first determine an average cloud-base height at which we extract vertical velocities ~~$w_b(x,y)$~~$w_b(x,y)$. This height corresponds to the altitude at which the average profile of condensed water reaches its first non-zero value. It is estimated at around 950 hPa on the two oceanic LES ~~(SAM and MesoNH)~~ and at around 750 hPa ~~on the LES for~~ for the LES of the AMMA case (~~MESONH)as seen in that shows the vertical profile of the horizontally averaged condensed water on the two cases~~cf. Fig. 4).

We then separate the updrafts on gust fronts from those associated with thermal plumes. Since the updrafts on gust fronts are both stronger and more coherent horizontally than ~~the thermals observed in the environment of cold pools~~those associated with thermal plumes, we define a gust front mask based on a threshold ~~on horizontally smoothed~~ applied to an horizontally moving average of the vertical velocity at cloud based ~~w_b (sliding~~

	$D_{\mathrm{wk}}(10^{-10}\ \mathrm{m}^{-2})$	σ_{wk}	σ_{gust}
RCE			
LES SAM	5	0.253	0.048
LES MESONH	5	0.264	0.017
AMMA			
LES MESONH	2.5	0.214	0.045

Table 1: Cold pools number density (D_{wk}), surface fraction of cold pools (σ_{wk}), and surface fraction of gust fronts (σ_{gust}) estimated from the LES for the RCE and AMMA cases. For the RCE case, the values represent an average over the 24 available time steps from the SAM LES and the 10 available time steps from the MESONH LES. For the AMMA case, the values are an average of the time steps obtained between 5:00 PM and 10:00 PM.

~~average over~~ w_b, denoted as $\tilde{w}_b(x,y)$. Because the gust fronts are stronger in the AMMA case than in the RCE case, different choices were made for the size of the horitontal box of the moving average (1.25 km×1.25 km for the RCE case and 2 km×2 km for AMMA~~)~~ ~~, denoted as $\tilde{w}_b(x,y)$ in the rest of the text. After several analyses, we selected a $\tilde{w}_b(x,y)$ thresholds of~~) and for the value of the vetrical velocity threshold (0.6 m/s for the RCE case and 2 m/s for the AMMA case~~to identify gust fronts~~). Those values were retained after several tests so as to separate as effectively as possible the gust front form other ascents.

~~Figure ?? presents~~ Fig. 5 and 6 overlays the updrafts within (red) and outside (green) gust fronts on maps of T_{10m} anomaly ~~, smoothed horizontally applying a sliding average on~~ (smoothed by applying a moving average with a box of 2.5 km×2.5 km), for the RCE and AMMA cases ~~. On these maps, we have overlaid the~~ respectively. The contours of the T_{10m} anomalies used to identify cold pools (-0.2 K for RCE and -1 K for AMMA) ~~, as wellas the updrafts on gust fronts (in red) and thermals (in green)~~ are displayed as well. Visually, the gust fronts computed with $\tilde{w}_b(x,y)$ thresholds of 0.6 m/s (RCE) and 2 m/s (AMMA) align well with the contours of cold pools identified using these T_{10m} anomaly thresholds. It also appears that most thermals are located in the environment of cold pools for both the RCE and AMMA cases~~()~~. This retrospectively validates a choice made in ~~version 6A of LMDZ~~ LMDZ6A, where the effect of thermals was only computed outside cold pools.

~~Finally, to determine ALE_{wk}, we take the maximum kinetic energy in the domain, considering only $w_b(x,y)$ in the gust fronts mask($w_{bgust}(x,y)$), as it is~~ Both ALE_{wk} and ALP_{wk} are computed from w_b restricted to the ~~maximum vertical velocity on the gust front that triggers convection. As for ALP_{wk}, which~~ gust front mask, noted $w_{b,gust}$.

ALE_{wk} is estimated as the kinetic energy associated with the maximum value of $w_{b,gust}(x,y)$:

$$ALE_{\mathrm{wk}} = \max(\frac{1}{2}{w_{b,gust}}^2) \tag{26}$$

ALP_{wk} represents the average updrafts power provided by all cold pools in the domain~~,~~

~~it is calculated from~~ . It is calculated as the horizontal average of the cube of w_{bgust} ~~,~~ ~~weighted by~~ times the surface fraction (σ_{gust}) covered by gust fronts~~. The mask applied to gust fronts was~~ :

$$ALP_{\mathrm{wk}} = \sigma_{gust}\frac{1}{2}\rho\overline{w_{b,gust}}^3 \tag{27}$$

. The gust front mask is used to calculate σ_{gust}, which is 0.048 (LES SAM) for the RCE case and 0.045 for the AMMA case, for the times shown in ~~figure ??.~~

$$\cancel{ALE_{wk} = max(\frac{1}{2}w_{bgust}^2)}$$

$$\cancel{ALP_{wk} = \sigma_{gust}\frac{1}{2}\rho\overline{w_{bgust}^3}}$$

Fig. 5 and 6. Characteristics of the cold pools estimated from the sampling are gathered on Table 1.

~~Values of density (D_{wk}), surface fraction of cold pools (σ_{wk}), and surface fraction of gust front (σ_{gust}) estimated from the LES for the RCE and AMMA cases. For the RCE case, the values represent an average over the 24 available time steps from the SAM LES and the 10 available time steps from the MESONH LES. For the AMMA case, the values are an average of the time steps obtained between 5:00 PM and 10:00 PM. $D_{wk}(10^{-10}$ m $^{-2})$ σ_{wk} σ_{gust} LES SAM 5 0.253 0.048 LES MESONH 5 0.264 0.017 LES MESONH 2.5 0.214 0.045~~

(a) and on the instant 7:30 PM of the LES of the AMMA case with black contours indicating thresholds of temperature at 10 m anomaly of -0.2 K (RCE) and -1 K (AMMA).

4.5 Validation of ~~Phenomenological Laws~~phenomenological laws

Physical parameterizations are defined by sets of mathematical equations ~~intended to represent the subgrid process~~ designed to represent subgrid processes within a column of the model. The formulation of these equations is based ~~on both~~ both on a phenomenological understanding of the processes ~~concerned and~~ involved and on fundamental principles of physics. These parameterizations can be ~~assessed in bulk, or piecewise~~evaluated as a whole or in parts, by isolating certain equations or ~~relations~~ relationships between internal variables, or between internal variables and ~~state variables of the GCM. LES offer~~ GCM state variables. LES offers the possibility of performing a priori validation and adjustment of these laws.

In the cold pool model, variables ~~ALE_{wk}, ALP_{wk}~~ ALE_{wk}, ALP_{wk} and C_* are determined from the collapse energy, $WAPE$ (see equations (4), (17) and (21)). We compare in ~~Table ??~~ Table 2 the values obtained using the parameterization formulations (parameterized value P), based on $WAPE$ deduced from $\delta\theta_v$, with those obtained directly from resolved wind in the LES (sampled value S): the vertical speed at cloud base (~~w_b) for~~

~~Vertical profile of condensed water averaged horizontally calculated at an instant of the LES (SAM and MESONH) of the RCE case and at 7:30 PM of the LES for the AMMA case.~~

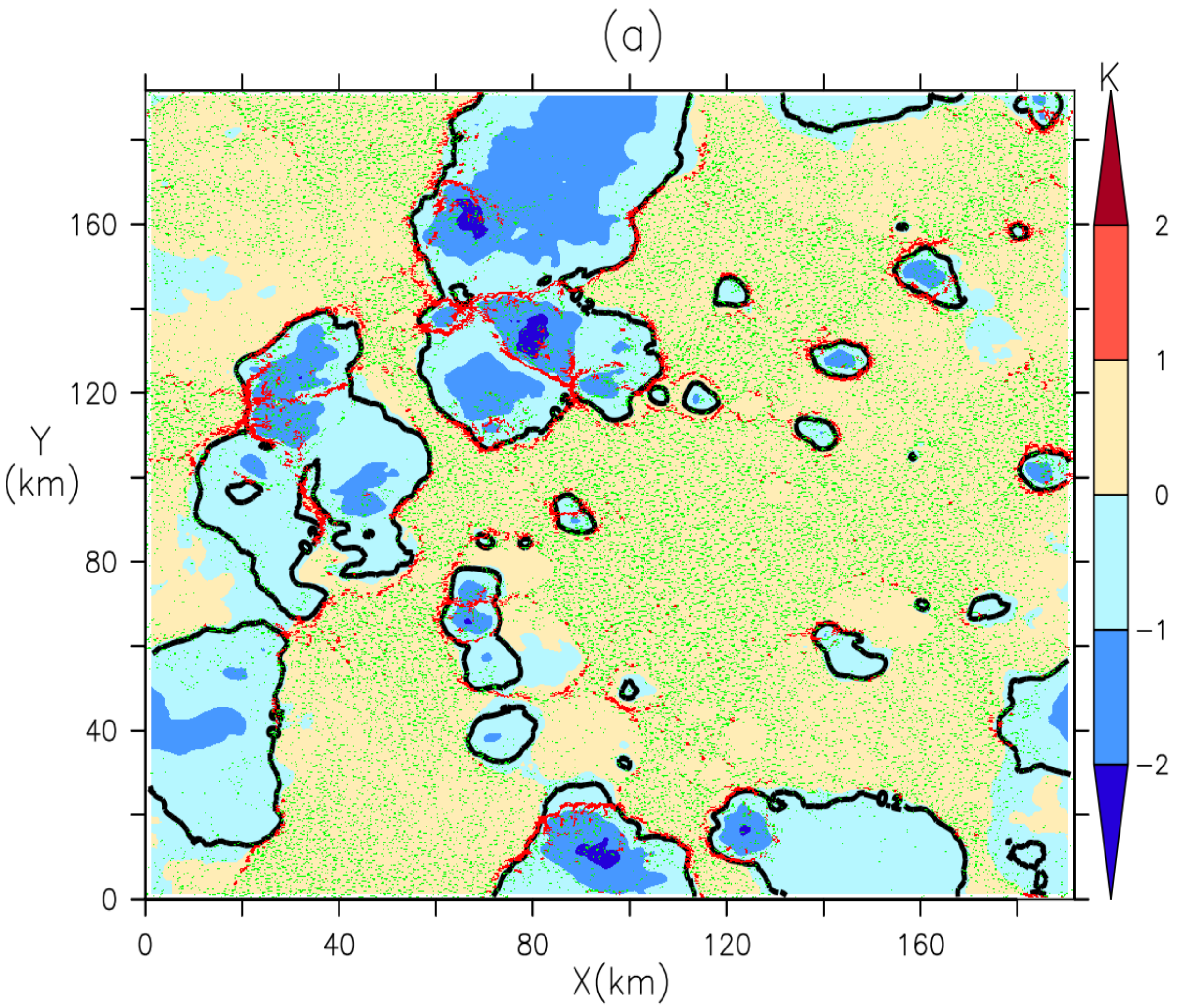

Figure 5: Map of T_{10m} anomaly (color shadings), smoothed (moving average with a horizontal box of 2.5 km×2.5 km), at an instant of the LES SAM of the RCE case. The black contour is the -0.2 K anomaly used to separate the inside from the environment of cold pools. The green and red dots show grid cells with vertical velocity at cloud base w_b larger than 0.8 m/s, inside (red) and outside (green) the gust front mask (see main text for the definition of the gust front mask).

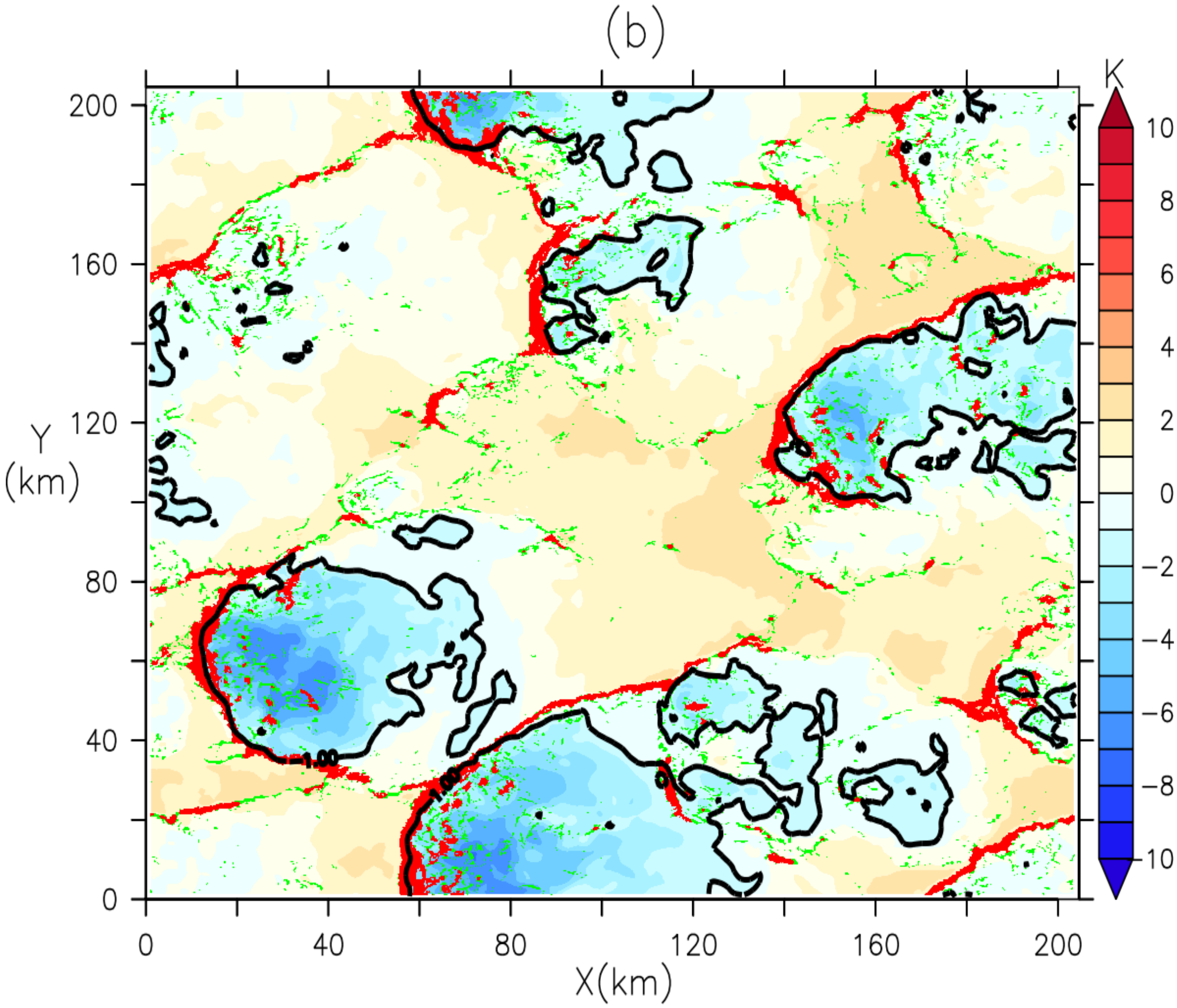

Figure 6: ~~Maps~~ Map of $T_{10\mathrm{m}}$ anomaly (color shadings), ~~with a sliding~~ smoothed (moving average with a horizontal box of 2.5 km×2.5 km), at ~~an instant of the LES SAM of the RCE case (a) and on the instant~~ 7:30 PM ~~of~~ for the LES of the AMMA case~~with~~. The black ~~contours indicating thresholds of temperature at 10 m anomaly of -0.2 K (RCE) and~~ contour is the -1 K ~~(AMMA)~~anomaly used to separate the inside from the environment of cold pools. The green and red ~~dotes indicates the updrafts on the gust fronts given by the~~ dots show grid cells with vertical ~~velocities~~ velocity at cloud base ~~(w_b) in the gust fronts mask. This mask is defined from a threshold value applied to the sliding average of w_b. For the RCE case, the average is done with a box of 1.25 km×1.25 km and values of $\tilde{w}_b > 0.6$ m s^{-1} are retained (respectively 2 km×~~w_b larger than 2 ~~km and $\tilde{w}_b > 2$~~ m~~-~~/s~~$^{-1}$ for AMMA). The~~, inside (red~~dotes are obtained by w_b ¿ 0.8 m s^{-1} for RCE~~) and ~~w_b ¿ 2 m s^{-1}. The~~ outside (green~~dots represent thermals, defined by w_b less than 0.8 m/s for~~) the ~~RCE case and 2 m/s~~ gust front mask (see main text for the ~~AMMA case, obtain generally outside cold pools~~definition of the gust front mask).

~~ALE_{wk} and ALP_{wk}~~w_b) for ALE_{wk} and ALP_{wk}, and the mean divergence of wind at 10 m in cold pools for C_*. These analyses are performed by averaging over the available time steps: 24 time steps for SAM and 7 for MESONH in the RCE case, and between 5:00 PM and 10:00 PM for the AMMA case.

The values of ~~ALE_{wk}~~ ALE_{wk} calculated by both methods are very close to each other. The largest error is an underestimation by about 30% of the ~~ALE_{wk}~~ ALE_{wk} computed from $WAPE$ compared to the w_{bgust} estimate. These results for the three LES confirm the validity of the hypothesis of equality between ~~ALE_{wk}~~ ALE_{wk} and $WAPE$ assumed in the parameterization.

~~Comparison of the variables $WAPE$, ALE_{wk}, C_* and ALP_{wk} obtained directly from the resolved wind in the LES (sampled values S), with those calculated using the formulations of the parameterization (parameterized values P). The S values are derived from the vertical velocity at cloud base (w_b) for ALE_{wk} and ALP_{wk}, from the mean divergence of wind at 10 m in cold pools for C_*, sampled directly from the LES. The P values are calculated from the $WAPE$ deduced from $\delta\theta_v$, itself sampled from the same LES, considering the coefficients k = 0.33 and k = 0.66. The analyses are based on the average of the available time steps: 24 time steps for the LES performed with SAM and 7 with MESONH in the oceanic RCE case, and between 5:00 PM and 10:00 PM for the LES of the AMMA case.~~

~~Table ??~~ Table 2 shows that, C_* values computed from the $WAPE$ are systematically lower than those coming from the mean divergence of wind at 10 m in cold pools. This difference could be due to an underestimation of the coefficient k, imposed here at 0.33. With ~~$k = 0.6$~~$k = 0.56$, the calculation of C_* based on the $WAPE$ becomes comparable to those obtained from the mean divergence of wind at 10 m in cold pools (~~table ??~~Table 2). As discussed above, the value of 0.33 was retained following an oral communication by Lafore (2000). But other studies propose different values: **?** estimate k at 0.68 based on CRM simulations of 2D squall grain, **?** estimate it at 0.5 from observations of cold pools during the BAMEX experiment in the American Great Plains. Our results are thus compatible with the hypothesis of the model which postulates that the kinetic energy of cold pools results from the transformation of $WAPE$ into kinetic energy with a coefficient k compatible with the published estimates.

~~Table ??~~ Table 2 also shows that, for the three LES cases, the values of ~~ALP_{wk}~~ ALP_{wk} calculated with $C*$ from $WAPE$ are at least three times lower than those obtained from w_{bgust}. Two coefficients are involved in the calculation of ~~ALP_{wk}~~ ALP_{wk} with the parameterization formula: the coefficient k and the lifting efficiency ϵ, imposed respectively to 0.33 and 0.25. Using k=~~0.66~~ 0.56 however in the calculation of C_*, and keeping ϵ at is nominal value of 0.25 allows to reconcile the various estimates. This is compatible with the hypothesis of the parameterization according to which 25% of the horizontal power provided by the cold pools during its propagation would be used to reinforce the intensity of the convection while a large part dissipates.

	$WAPE$ (J/Kg)	~~ALE_{wk}~~ $ALE_{\mathbf{wk}}$ (J/kg) (S)	C_* (m/s) (P) k=0.33	C_* (m/s) (S)	C_* (m/s) (P) k=~~0.66~~ 0.56	~~ALP_{wk}~~ $ALP_{\mathbf{wk}}$ (J/kg) (P) k=0.33	~~ALP_{wk}~~ $ALP_{\mathbf{wk}}$ (W/m^2) (S)	~~ALP_{wk}~~ $ALP_{\mathbf{wk}}$ (W/m^2) (P) k=~~0.66~~ 0.56
RCE SAM	7.962	10.460	1.315	2.228	~~2.630~~ 2.232	0.008	0.054	~~0.071~~ 0.044
RCE MESO	7.912	6.965	1.313	2.264	~~2.625~~ 2.228	0.008	0.020	~~0.071~~ 0.044
AMMA MESO	45.870	59.760	3.133	5.362	~~6.265~~ 5.316	0.279	1.733	~~2.239~~ 1.368

Table 2: Comparison of the variables $WAPE$, ALE_{wk}, C_*, and ALP_{wk} obtained directly from the resolved wind in the LES (sampled values S), with those calculated using the formulations of the parameterization (parameterized values P). The S values are derived from the vertical velocity at cloud base (w_b) for ALE_{wk} and ALP_{wk}, from the mean divergence of wind at 10 m in cold pools for C_*, sampled directly from the LES. The P values are calculated from the $WAPE$ deduced from $\delta\theta_v$, itself sampled from the same LES, considering the coefficients k = 0.33 and k = 0.56. The analyses are based on the average of the available time steps: 24 time steps for the LES performed with SAM and 7 with MESONH in the oceanic RCE case, and between 5:00 PM and 10:00 PM for the LES of the AMMA case.

5 Evaluation in the single column configuration of LMDZ

In this section, we evaluate the cold pool parameterization in the SCM configuration of LMDZ. The comparison is more demanding here, since all parameterizations interact with each other and because the state of the atmosphere at the time of evaluation depends on the interaction of all those parameterizations during the preceeding hours (AMMA) or days (RCE). The SCM simulations are performed with exactly the same initial and boundary conditions as the corresponding LES for both cases.

For the RCE case, we represent diagnostics once a quasi-steady state has been reached by averaging results between day 40 and 44.

In the AMMA case, cold pools appear around 5:00 PM in the LES but as early as 1:30 PM in LMDZ CTRL, revealing a model limitation. Adjusting the S_{trig} parameter could delay this onset, though a more physical approach would be required. For comparison, we focus on the times when cold pools are most developed: 7:30 PM in the LES and 2:30 PM in LMDZ CTRL, where the intermediate analysis of δT shows colder and thus more pronounced pools.

In order to facilitate comparisons between LMDZ and LES, we also impose in the LMDZ simulations the density of cold pools estimated in the LES. We thus set a density of 5 cold pools per 100 km$\times$100 km, both for the RCE and AMMA cases. To represent the profiles of δT, δq and δw in LMDZ CTRL for the RCE case, we perform a time average between the 41st and 43rd day of simulation, in order to compare with the LES at the same times. For the AMMA case, the analysis is performed at 7:30 PM in the LES and at 2:30 PM in LMDZ CTRL, as specified above. The same procedure is applied to compare the $WAPE$, ALE, and ALP variables between LMDZ CTRL and the LES for both cases.

5.1 Vertical profiles of δT, δq and δw

The analysis of the δT profiles in the LES confirms that cold pools are colder at the surface with temperatures increasing towards the top for the three LES. The cold pools are about three times deeper in AMMA (Fig. 7a) than for the RCE case (Fig. 7d). In the LES, it is observed that the cold pool temperatures for the AMMA case (around –4 K) are lower than those of the RCE case (around –1.2 K)~~, which remains~~. This is consistent with observations ~~, although the latter generally~~ which indicate much colder pools over land than over the ocean. For the AMMA case in particular, observations reveal a temperature drop of approximately –5 K during the passage of the cold pool (**?**), a value fairly close to that ~~simulated by~~ of the LES. It should ~~also be noted~~ be noted however that the AMMA case corresponds to a ~~particularly weak and atypical~~ relatively weak episode of continental convection. The δq profiles indicate that at the surface, cold pools are wetter than the surrounding air in the RCE case and the AMMA case (~~b and~~ Fig. 7b and 7e). In both cases, the excess of humidity within cold pools decreases with altitude ~~until they reach their summit, where they are dried by the subsidence~~ up to the cold pools top. The humidity

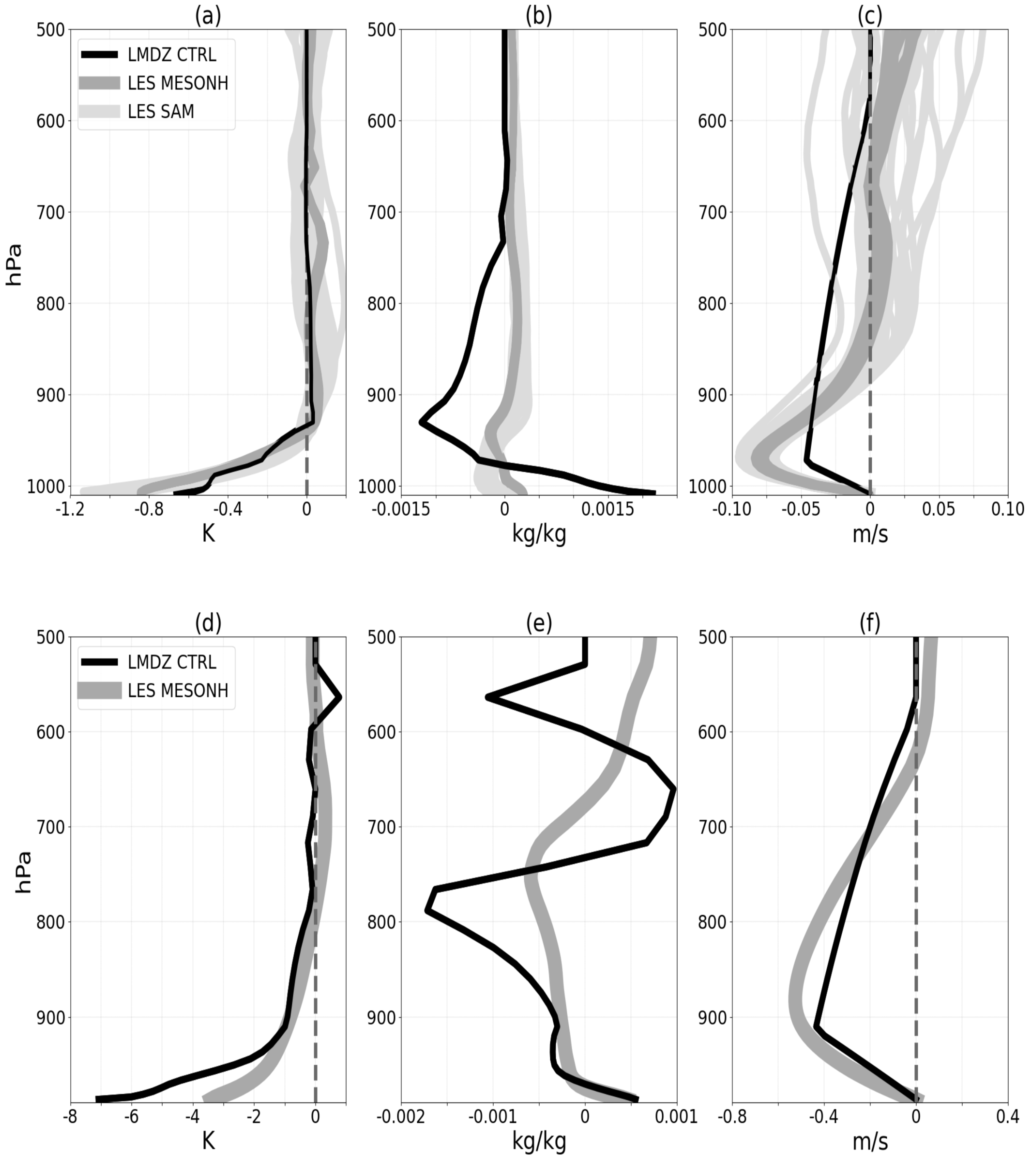

Figure 7: Vertical profiles of δT, δq and δw calculated in the LES and simulated by LMDZ control (LMDZ CTRL)~~on~~. For the RCE case (a, b, c)~~and on the AMMA case (d, e, f). For the RCE case~~, the profiles are shown for a set of 24 ~~and 10 instants respectively~~ times for ~~LES~~ the SAM LES (light grey) and ~~MESONH, while those~~ 10 for MESONH (dark grey). For LMDZ CTRL~~represent a average over days 41, 42~~, ~~and~~ results are averaged from day 41 to 43. For the AMMA case (d, e, f), the profiles correspond to the times when cold pools were most developed, i.e., 7:30 PM in LES and 2:30 PM in LMDZ CTRL.

	$WAPE$ (J/Kg)	~~ALE_{wk}~~ $ALE_{\mathbf{wk}}$ (J/kg)	C_* (m/s)	~~ALP_{wk}~~ $ALP_{\mathbf{wk}}$ (W/m^2)
		RCE		
LES SAM	7.962	10.460	2.228	0.054
LES MESONH	7.912	6.965	2.264	0.020
LMDZ CTRL	2.957	2.957	0.802	0.001
		AMMA		
LES MESONH	62.110	66.960	4.762	2.304
LMDZ CTRL	71.300	75.170	3.941	0.103

Table 3: Comparison of the $WAPE$, $ALE_{\mathbf{wk}}$, C_* and $ALP_{\mathbf{wk}}$ computed from sampling of the LES and by LMDZ control (LMDZ CTRL) for the RCE case and the AMMA case. For the RCE case, comparisons are made using an average of the days following the achievement of equilibrium (days 41, 42, and 43). For the AMMA case, they are performed at the times when the cold pools are most developed (7:30 PM in the LES and 2:30 PM in LMDZ CTRL).

deficit above this level is due to the lateral entrainment of dry air ~~masses into~~ from the mid troposphere and its subsidence into the cold pools (~~c and ??~~Fig. 7c and 7f). ~~On~~ For the RCE case, this subsidence vanishes below 800 hPa (Fig. 7c), while for the AMMA case, it vanishes at a higher level, around 600 hPa (Fig. 7f).

The δT profiles simulated with LMDZ CTRL are qualitatively consistent with LES, with a cold pool top (where δT ~~cancelled~~cancels) at about the right altitude. Cold pools simulated with LMDZ are however warmer than in the LES for the RCE case (Fig. 7a), and colder at the surface than the LES for the AMMA case (Fig. 7d). Consistently with LES, cold pools are also wetter at the surface and drier close to their top top (~~b and~~ Fig. 7b and Fig. 7e). However the variations of δq are much larger in LMDZ than in the corresponding LES. In particular, the cold pools are much too dry at their top in LMDZ. In both cases, cold pools are associated with subsidence. The height at which the subsidence of air masses in cold pools begins, fixed at 600 hPa in LMDZ CTRL, is too high compared to LES for the RCE case ~~??~~(Fig. 7e).

The comparisons also reveal that the model simulates wetter cold pools at the surface than those in the LES in both cases, with a more pronounced difference for the RCE case.

5.2 WAPE, ALE and ALP

~~Comparison of the $WAPE$, ALE_{wk}, C_* and ALP_{wk} computed from sampling of the LES and by LMDZ control (LMDZ CTRL) for the RCE case and the AMMA case. For the RCE case, comparisons are made using an average of the days following the achievement of equilibrium (days 41, 42, and 43). For the AMMA case, they are performed at the times when the cold pools are most developed (7:30 PM in the LES and 2:30 PM in LMDZ CTRL).~~

For the RCE case, the $WAPE$ is significanlty smaller in LMDZ CTRL than in the

Simulations	**Protocols**
LMDZ CTRL	simulation of LMDZ with the standard configuration except that D_{wk} to 5 per 100×100 km^2 for the RCE case and 2.5 for AMMA
LMDZ ~~(CTRL,~~ V1 ~~,~~	LMDZ CTRL + change of k to 0.56
LMDZ V2 ~~,~~	LMDZ V1 + changed computation of p_{upper}
LMDZ V3 ~~).~~	LMDZ V2 + activation of thermals throughout the domain

Table 4: Description of simulations performed with LMDZ in the standard configuration and with various modifications

LES, with a difference of at least a factor of 2 (~~Table ??~~Table 3). These low values of $WAPE$ in LMDZ CTRL also translate into low ~~ALE_{wk}~~ ALE_{wk} values compared to LES (~~table ??~~Table 3). On the other hand, for the AMMA case, the $WAPE$ simulated by the model, and consequently ~~ALE_{wk}~~ALE_{wk}, are slightly higher than the values derived from the LES (~~Table ??~~Table 3). The value of C_* simulated by LMDZ CTRL is at least three times smaller than that of the LES in the RCE case and slightly lower for the AMMA case (~~Table ??). ALP_{wk}~~ Table 3). ALP_{wk} is at least twenty times weaker in LMDZ CTRL than in the LES for all cases (~~Table ??~~Table 3).

~~Several discrepancies have been identified between the parameterized cold pools and the one sampled in the LES, in particular they are too wet near the surface and too dry at their top associated with a subsidence starting too high, at least in the RCE case. The $WAPE$, ALE_{wk}, C_*, ALP_{wk} are globally underestimated.~~ Various modifications of the cold pool parameterization are explored in the following section to ~~improve the model behavior~~try to correct the defects listed above.

6 Improvements of cold pool model

Here, we start by correcting the identified discrepancies between the LES and the model concerning the value of the coefficient k and the ~~altitude h_m~~pressure height p_{upper}, and by assessing the impact of these changes on the temperature and humidity difference between the cold pools and their environment, before exploring other avenues for improvement.

6.1 Coefficient k

[A relier en detail si on decide de prendre k=0.56 plutot que k=0.66 et que ca change les resultats pour V1,]

We present here the impact of increasing the coefficient k from 0.33 to ~~0.66~~ 0.56 (LMDZ V1 simulation) on the profiles of δT, δq, δw as well as on the variables C_*, $WAPE$, ~~ALP_{wk} and ALE_{wk}~~ALP_{wk} and ALE_{wk} (see Table 4). In the RCE case, this modification significantly improves the profile of δw below ~~h_{wk} (~~p_{wk} (Fig. 8c). It also allows for a

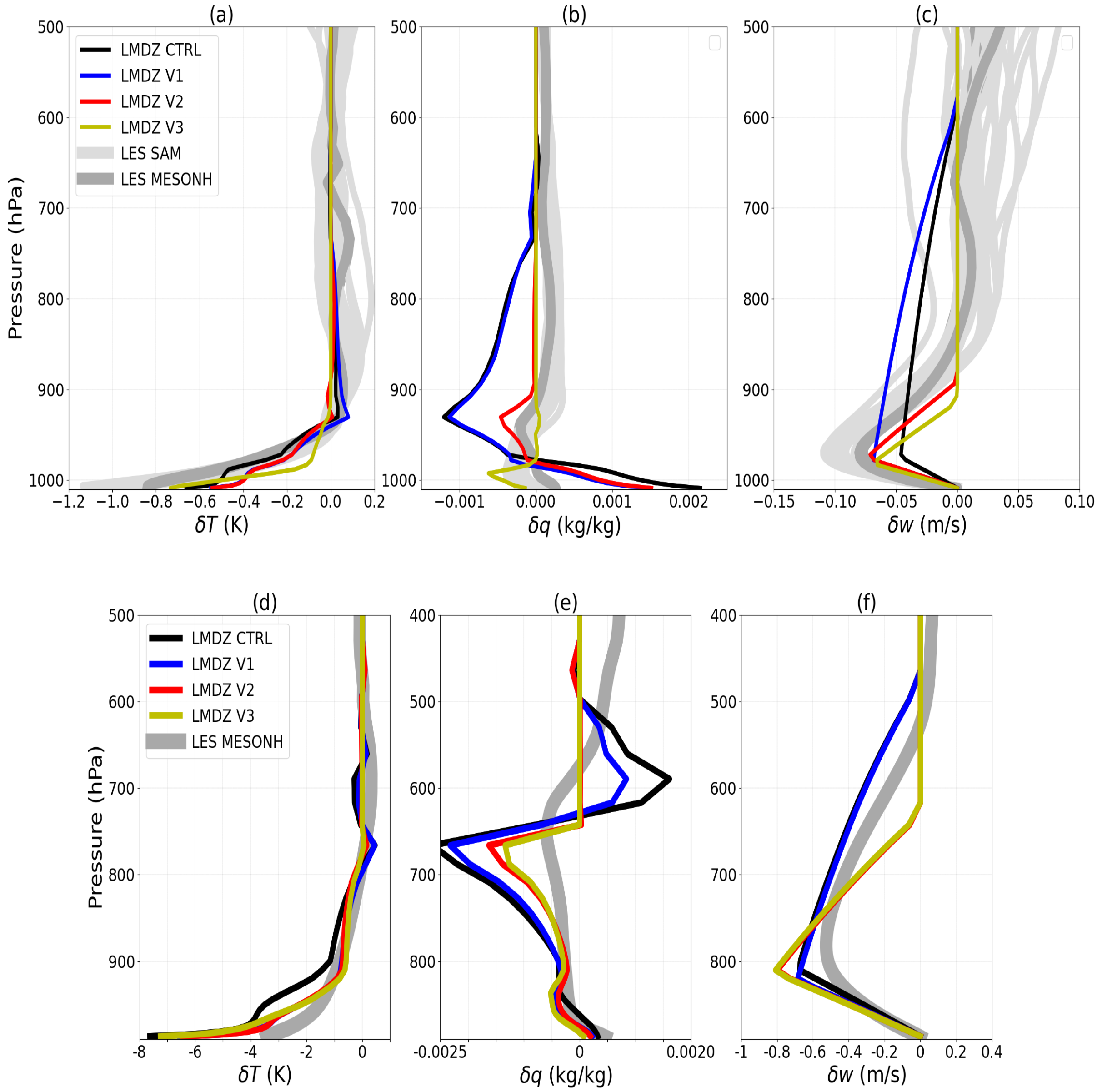

Figure 8: Vertical profiles of δT, δq and δw calculated in the LES and simulated ~~in the control~~ with LMDZ: for a control simulation (CTRL, same curves as Fig. 9), ~~LMDZ~~ with ~~the~~ adjustment of the coefficient k to ~~0.66~~ 0.56 (V1), ~~LMDZ~~ with the ~~drop in altitude (h_m) at which the subsidence~~ modified computation of ~~the air masses in cold pools is zero~~ p_{upper} (V2) and ~~LMDZ~~ with the activation of thermals in the entire domain (V3)~~on~~. Both the RCE ~~case~~ (a, b, c) and ~~on the~~ AMMA ~~case~~ (d, e, f) ~~. For the RCE case, the profiles~~ cases are shown for ~~a set of 24 and 10 instants respectively for LES SAM and MESONH, while those for LMDZ (CTRL, V1, V2, V3) represent a average over days 41, 42, and 43. For the AMMA case, the profiles correspond to~~ the times ~~when cold pools were most developed, i.e., 7:30 PM in LES and 2:30 PM~~ as in ~~LMDZ (CTRL, V1, V2, V3)~~ Fig. 9.

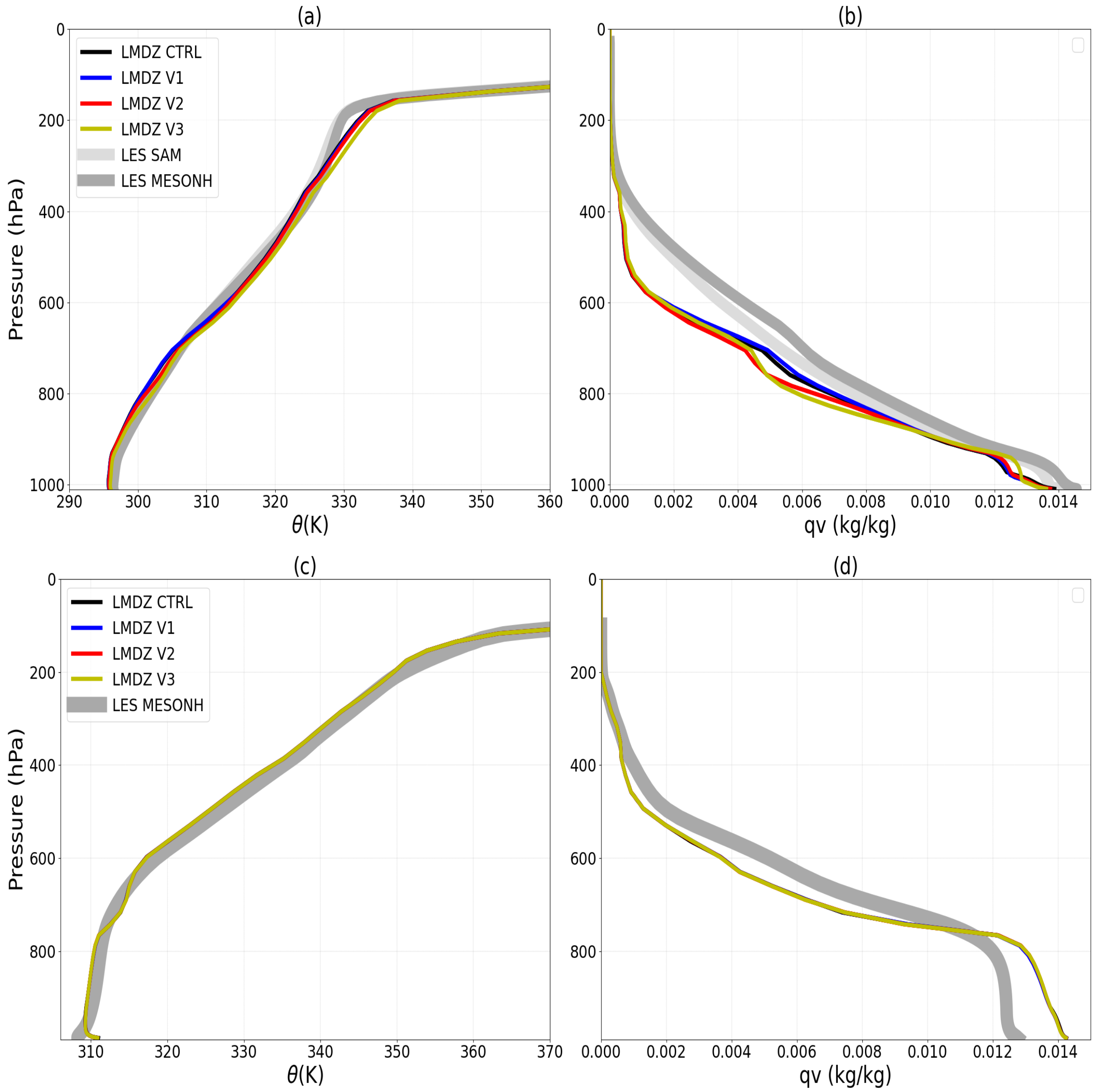

Figure 9: Vertical profiles of potential temperature (θ) and specific humidity (qv) calculated in the LES and simulated ~~in control~~ with LMDZ: for a control simulation (~~LMDZ~~ CTRL), ~~LMDZ~~ with ~~the~~ adjustment of the coefficient k to ~~0.66~~ 0.56 (V1), ~~LMDZ~~ with the ~~drop in altitude (h_m) at which the subsidence~~ modified computation of ~~the air masses in cold pools is zero~~ p_{upper} (V2) and ~~LMDZ~~ with the activation of thermals in the entire domain (V3)~~on~~. Both the RCE ~~case~~ (a, b) and ~~on the~~ AMMA ~~case~~ (c, d) ~~. The LES profiles correspond simply to horizontal averages over the full domain. For the RCE case, the profiles~~ cases are shown for ~~a set of 24 and 10 instants respectively for LES SAM and MESONH, while those for LMDZ (CTRL, V1, V2, V3) represent a average over days 41, 42, and 43. For the AMMA case, the profiles correspond to~~ the same times ~~when cold pools were most developed, i.e., 7:30 PM in LES and 2:30 PM~~ as in Fig. 9.

better representation of the δw profiles below ~~h_{wk}~~ p_{wk} in the AMMA case (Fig. 8f). These improvements are directly linked to the increase in C_* for both cases (~~Table ??~~Table 5), since the δw profile below ~~h_{wk}~~ p_{wk} depends on the spreading of cold pools. The increase in C_* could be associated with stronger air mass subsidence within the cold pool, which would contribute to a slight drying near the surface in both cases (~~Fig. ??b and Fig. ??~~Fig. 8b and 8e). For the AMMA case, this drying results in cold pools that are slightly drier at the surface in LMDZ V1 than in the LES, but they remain overall comparable to the latter. The increase in C_* in both the RCE and AMMA cases also leads to a better representation of ~~ALP_{wk}~~ ALP_{wk} (an increase by at least a factor of 5 for both cases), even though this variable remains underestimated (~~Table ??~~Table 5). We also note a warming effect from this modification in both the RCE and AMMA cases. The impact on the δT profiles in the AMMA and RCE cases is responsible for the decrease in the values of $WAPE$ and ~~ALE_{wk}~~ ALE_{wk} for these two cases (~~Table ??~~Table 5).

Fig. 9 shows that the modification introduced in version V1 has a low impact on the θ and qv mean profiles (Fig. 9), the black and blue curves being almost superimposed. Both CTRL and V1 simulations reproduce the θ profiles fairly well. Around 600 hPa, the temperature is too warm in the RCE case. Regarding humidity, a dry bias is present in the boundary layer in the RCE case, as well as between 800 and 400 hPa. For the AMMA case, there is a wet bias in the boundary layer and above 600 hPa, and a dry bias between 700 and 600 hPa.

6.2 ~~Altitude h_m~~ Choice of cold pools scheme upper bound, p_{upper}

In the previous sections, we found that the altitude at which the subsidence of dry air above cold pools initiate is located around 800 hPa in the LES for the RCE case and around 600 hPa for the AMMA case, while in LMDZ, ~~this altitude h_m~~ p_{upper} is arbitrarily set to 600 hPa in the original version of the parameterization. In version V2, in addition to the change of the value of k from 0.33 to ~~0.66, we compute h_m as αh_{wk} with $\alpha = 3$ (α~~ 0.56, we impose $p_{\mathrm{srf}} - p_{\mathrm{upper}} = \gamma_{\mathrm{wk,upper}}(p_{\mathrm{srf}} - p_{\mathrm{wk}})$ with $\gamma_{\mathrm{wk,upper}}$, fixed here to 3, is considered as a new free parameter in the following section~~)~~.

A slight adjustment of ~~h_{wk}~~ p_{wk} was also made thanks to the new numerical scheme proposed for its calculation, although the details are not discussed here. This adjustment, however, has no impact on the vertical profiles of δT, δq.

Comparisons between LMDZ V2 simulations and LES show a better representation of the δq profiles at the top of cold pools in both the RCE and AMMA cases (~~b and~~ Fig. 8b and 8e). These results show that the dry bias at the top of the cold pool in the original version was due to advection of dry air from too high an altitude. This modification also reduces slightly the humidity of cold pools near surface in the RCE case, although they remain more humid than in the LES.

Note finally that this modification has a very limited impact on the δT profiles.

~~Table ??~~ Table 5 shows that the ~~decrease in h_m~~ change in p_{upper} weakly affects the variables $WAPE$, C_*, ~~ALE_{wk} and ALP_{wk}~~ ALE_{wk} and ALP_{wk} for these two cases.

Versions V2 does not modify much the mean vertical profiles except for a drying of the mid-troposphere in the RCE case (Fig. 9b), in a region where the CTRL simulation was already to dry. Although the time evolution of the mean profiles is the first target of physics parameterizations, we think however that the improvement of the internal variables is so strong for this modification that it should be adopted in the future in LMDZ.

6.3 Activation of thermals throughout the domain

~~In~~ As explained above, in the standard LMDZ configuration, thermals only interact with temperature and humidity profiles outside cold pools~~.~~, inducing a differential heating in moistening (equation (7)). This choice was originally made to account for the fact that the atmosphere is more stable inside cold pools, and indeed the analysis above shows that the thermal plumes that reach cloud base are essentially located outside cold pools. ~~As a result of this choice, the boundary layer convection is reinforced, and an additional term is added to the time evolution of the cold pool temperature and humidity anomalies .~~ Version V3 is identical to version V2, except that we consider that thermal plumes ~~interact with the mean grid cellprofiles, with no effect of thermal plumes on the temperature and humidity cold pool anomalies~~are active everywhere in the grid cell. Consistently, the terms ${Q_1}^{\mathrm{th}}$ and ${Q_2}^{\mathrm{th}}$ are removed from (7). For the RCE case, this leads to a decrease in the surface humidity of cold pools, closer to the LES results (Fig. 8b). In the AMMA case, the effect is also present, although less pronounced (~~Fig. ??~~Fig. 8e). This result is expected because the vertical transport by thermals systematically dries the surface (**?**). This confirms the key role of boundary layer convection in regulating surface humidity on both continent (**?**) and ocean (**?**), via the mixing of moist air with dry air above.

One way to improve the representation of humidity anomaly profile without activating the thermal plumes everywhere would be to add a simple parameterization of shallow and cloud-free boundary layer convection (a simplified version of the thermal plume model) within the cold pool.

~~Tests not shown allowed to assess the impact of surface evaporation flux on cold pool moisture by activating splitting, which differentiates this flux between (w) and (x). In the standard configuration, this flux is treated uniformly for both regions. The tests showed a limited effect of this flux on cold pools moisture for RCE. This test was not carried out for AMMA, as LMDZ does not yet allow it on the continent. However, it would be relevant to explore it.~~

In version V3, cold pools are colder than in version V2 in ~~the RCE case ant the AMMA case (Fig. ??a and Fig. ??d~~both the RCE and AMMA cases (Fig. 8). In the RCE case, however, cold pools remain less cold than in the LES despite this effect. In the AMMA case, this cooling accentuates the overestimation of the cold anomaly. In both cases, this cooling leads to an increase in the $WAPE$, C_*, ~~ALE_{wk}, and ALP_{wk} variables (Table ??).~~ ALE_{wk}, and ALP_{wk} variables (Table 5).

Version V3 does not introduce any notable changes, compared to V2, in the profiles of θ and q_v for the RCE and AMMA cases.

	$WAPE$ (J/Kg)	~~ALE_{wk}~~ $ALE_{\mathbf{wk}}$ (J/kg)	C_* (m/s)	~~ALP_{wk}~~ $ALP_{\mathbf{wk}}$ (W/m^2)
		RCE		
LES SAM	7.962	10.460	2.228	0.054
LES MESONH	7.912	6.965	2.264	0.020
LMDZ CTRL	2.957	2.957	0.802	0.001
LMDZ V1	~~2.528~~ 2.663	~~2.528~~ 2.663	~~1.484~~ 1.292	~~0.006~~ 0.004
LMDZ V2	~~2.465~~ 2.620	~~2.465~~ 2.620	~~1.465~~ 1.282	~~0.006~~ 0.004
LMDZ V3	~~3.408~~ 3.585	~~3.408~~ 3.585	~~1.723~~ 1.500	~~0.009~~ 0.0055
12 bests	[5.1,5.3]	[5.1,5.3]	[1.79,1.83]	[0.013,0.025]
		AMMA		
LES MESONH	62.110	66.960	4.762	2.304
LMDZ CTRL	71.300	75.170	3.941	0.103
LMDZ V1	~~51.550~~ 56.930	~~51.100~~ 56.930	~~6.701~~ 5.975	~~0.538~~ 0.234
LMDZ V2	~~54.940~~ 57.990	~~53.550~~ 57.990	~~6.918~~ 6.031	~~0.732~~ 0.252
LMDZ V3	~~55.450~~ 58.190	~~53.260~~ 58.190	~~6.951~~ 6.041	~~0.756~~ 0.334
12 bests	[40,60]	[40,60]	[4.5,5.1]	[0.5,2.5]

Table 5: Comparison of the variables $WAPE$, $ALE_{\mathbf{wk}}$, C_* and $ALP_{\mathbf{wk}}$ calculated from the samplings in the LES, with those obtained with LMDZ: in a control simulation (CTRL), with the adjustment of the coefficient k to 0.56 (V1), with the modified computation of p_{upper} (V2), the activation of thermals in the entire domain (V3) and for the 12 best simulations of a tuning experiment, for the RCE and AMMA cases.

~~Description of simulations performed with LMDZ in the standard configuration and with various modifications~~ ~~**Simulations Protocols**~~ ~~LMDZ CTRL simulation of LMDZ with the standard configuration by imposing D_{wk} to 510^{-10} LMDZ V1 LMDZ CTRL + change of k to 0.66 LMDZ V2 LMDZ V1 + drop of h_m LMDZ V3 LMDZ V2 + activation of thermals throughout the domain~~

~~Comparison of the variables $WAPE$, ALE_{wk}, C_* and ALP_{wk} calculated from the samplings in the LES, with those simulated in LMDZ control (LMDZ CTRL), LMDZ with the adjustment of the coefficient k to 0.66 (V1), LMDZ with the drop in altitude (h_m) at which the subsidence of the air masses in cold pools is zero (V2) and LMDZ with the activation of thermals in the entire domain (V3) on the RCE case and on the AMMA case.~~

6.4 Tuning of free parameters

The tests presented above show possible avenues for improving the cold pool parameterization. However, we see that the modifications do not sufficiently affect the mean profiles to reduce these biases significantly. All tests underestimate (for the RCE case) or overestimate (for the AMMA case) the cold temperature anomaly inside cold pools, as well as $WAPE$, $\cancel{ALE_{wk}}$$ALE_{\mathrm{wk}}$, C_*, and $\cancel{ALP_{wk}}$$ALP_{\mathrm{wk}}$. We also observe systematic errors in the mean profiles, notably profiles that are much too dry for the RCE case.

In the GCM, these variables are not sensitive only to the parameters or formulation of the cold pool model. They are influenced by all other parameterizations, and in particular by the convection scheme to which the cold pool scheme is strongly coupled. In an attempt to see how modifications to other parameterizations could help reduce these biases, we performed automatic calibration simulations using the htexplo tool.

In practice, we decided to start from a tuning performed for the convective boundary layer by **?**, for a configuration with 95 levels rather than 79 and using more recent versions of the codes than those used in the rest of the chapter. This version indeed serves as the basis for preparing the future version of the climate model for the FastTrac part of the CMIP7 project, whose simulations are scheduled to begin in early 2026. We assume that the boundary layer parameters have already been optimized to accurately represent the convective boundary layer and associated clouds, cumulus and stratocumulus.

~~Metrics (targets and 1-σ tolerances) used for the tuning. For the RCE case, they concern the averages between days 41 and 43 of the WAPE and the cold pool spreading rate C_*, as well as the vertical profiles of $\delta\theta$, qv, and θ averaged over the altitude ranges specified in the right column. For the AMMA case, only the WAPE averaged between hours 10 and 17 of the simulation is used.~~

~~We target metrics preferentially on the RCE case. Indeed, we wish to avoid being overly dependent on errors in the phasing of the deep convective diurnal cycle.~~

~~For the RCE case, we target the quasi-equilibrium phase by considering averages between days 41 and 43. The metrics selected for these calibration exercises are the profiles of δT, q_v, and θ, evaluated from vertical averages at different levels and from temporal averages between days 41 and 43 as indicated in Table **??**. Free parameters considered in the tuning exercise.~~

Regarding modifications to the cold pool model, those affecting the coefficient k and $\cancel{h_m}$ p_{upper} were taken into account, as in the V2 configuration. Adjustments related to thermals (V3) are not considered here because they raise as many questions as they solve.

The tuning is performed using the `htexplo` tool as explained in Appendix A. We choose metrics preferentially on the RCE case targeting the WAPE, ALP and the profiles of anomalies and mean variables. Indeed, we wish to avoid being overly dependent on errors in the phasing of the deep convective diurnal cycle. The adjustable parameters selected for the cold pool model are: k, $\cancel{h_m}$$\gamma_{\mathrm{wk,upper}}$, σ_{int}, and ϵ. ~~The following parameters for deep convection~~ Parameters involved in the deep convection scheme are also included: the minimum wb_{srf} and maximum wb_{max} vertical velocities at the base of the convective column; the fraction of the grid cell area in which precipitating downdrafts occur, σ_{desc}; and the maximum precipitation efficiency in the Emmanuel scheme ($EP_{\max}$). This efficiency is a maximum efficiency at the top of the convective columns. The difference 1-$EP_{\max}$ controls how much condensed water exits the convective clouds, and thus the moisture source in the upper atmosphere. Details on the metrics and parameter ranges chosen are given in Appendix A.

The result of this tuning is the product of extensive trial and error regarding the choice of parameters, their bounds, the metrics to adjust, and the associated tolerances. We present here the 12 best simulations resulting from 13 waves of tuning. Among them, the simulation considered to be the most performant (TUNE BEST) is also identified.

The analysis of the results for the RCE case reveals that the simulations improve the representation of the targeted variables, particularly the mean humidity ~~profiles~~ profile and the amplitude of the potential temperature deviations $\delta\theta$. These deviations are more negative, consistent with a stronger WAPE and C_* coefficient. Furthermore, the δq profiles at the top of the cold pools, as well as the δw profiles, remain well represented across all 12 simulations ~~.~~

By applying the parameters from the tuning performed on the RCE case to the AMMA case simulations, a significant reduction in the cold bias at the surface of cold pools is observed (~~Fig. ??~~Fig. 10d), as well as an improvement in the mean humidity profiles across all 12 simulations. Only the results from the BEST TUNE simulation reproduce δq and δw profiles consistent with the LES, the others tending to generate cold pools that are too dry at the top due to slightly overestimated δw profiles (~~Fig. ??e and Fig. ??~~Fig. 10e and 10f). The BEST TUNE simulation also provides a better representation of $WAPE$ (~~Fig. ??~~Fig. 12a) and ~~ALP_{wk} (Fig. ??~~ALP_{wk} (Fig. 12b) in the AMMA case, with values very close to those from the LES at the time when cold pools reach their maximum development (~~Table ??)~~Table 5), despite a shift by about 3 hours earlier in the afternoon. Nevertheless, a moist bias and a cold bias persist in the boundary layer.

~~Same as Table ??, but including the 12 best tuning simulations. $WAPE$ (J/Kg) ALE_{wk} (J/kg) C_* (m/s) ALP_{wk} (W/m^2) LES SAM 7.962 10.460 2.228 0.054 LES MESONH 7.912 6.965 2.264 0.020 LMDZ CTRL 2.957 2.957 0.802 0.001 LMDZ V1 2.528 2.528 1.484 0.006 LMDZ V2 2.465 2.465 1.465 0.006 LMDZ V3 3.408 3.408 1.723 0.009 12 bests 5.1,5.35.1,5.31.79,1.830.013,0.025LES MESONH 62.110 66.960 4.762 2.304 LMDZ CTRL 71.300 71.300 3.941 0.103 LMDZ V1 51.550 51.100 6.701 0.538 LMDZ V2 54.940 54.940 6.918 0.732 LMDZ V3 55.450 55.450 6.951 0.756 12 bests 40,6040,604.5,5.10.5,2.5~~

7 Conclusions

Although the cold pool model proposed by **?** has improved the representation of convection in the LMDZ climate model **?**, its internal variables and physical properties had never been evaluated in details so far. This work proposes, for the first time, a detailed evaluation of the cold pool model, based on LES. We evaluate both the physics of the model, its internal variables and those involved in the coupling with deep convection, based on two oceanic LES in the RCE regime and a continental LES of the AMMA case. ~~We introduced~~

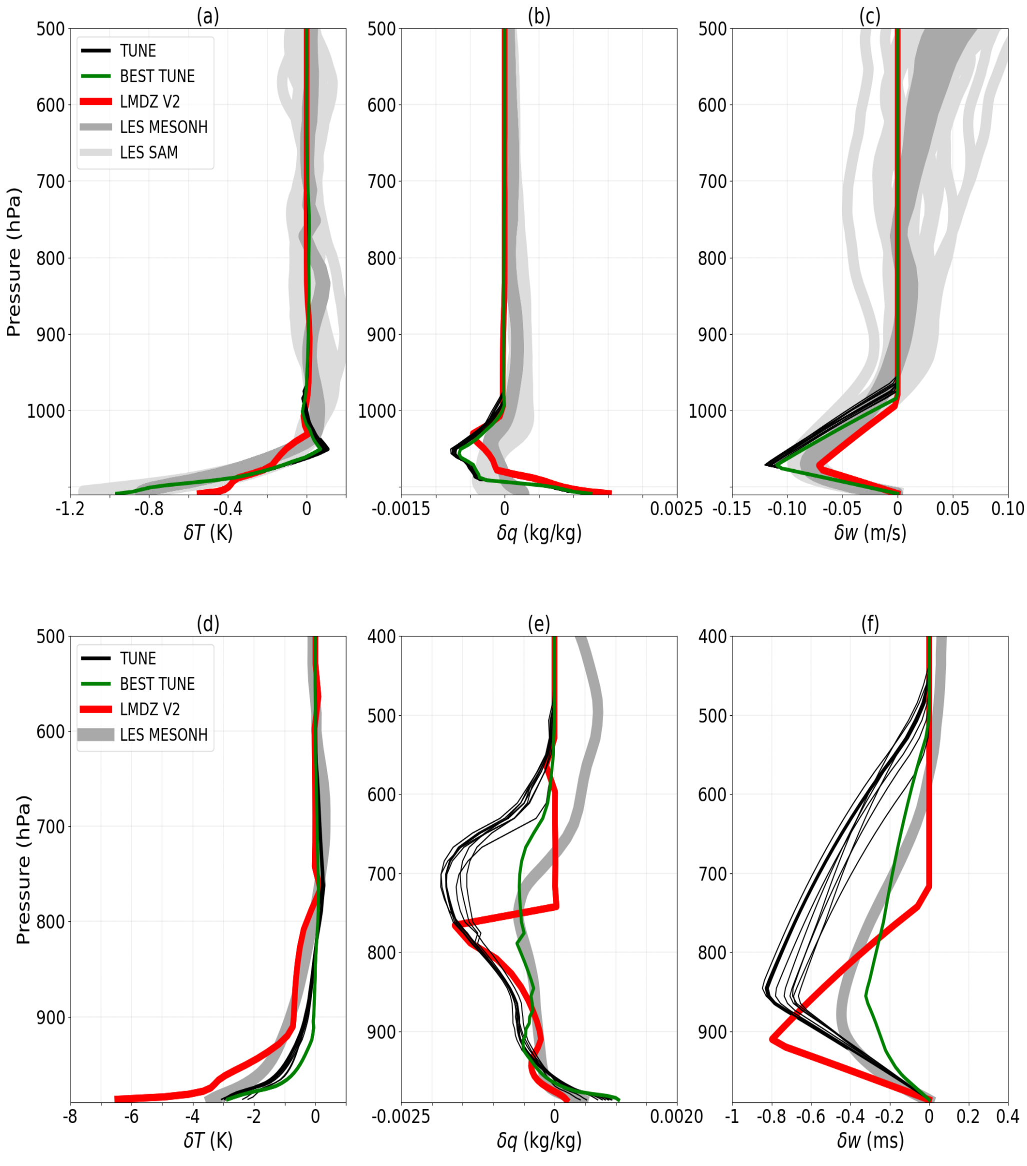

Figure 10: Like ~~Fig. ??~~Fig. 8, but ~~including~~ showing for LMDZ, the V2 simulation, the 12 best simulations from the tuning (TUNE, in black) as well as the best one among them (TUNE BEST, in green).

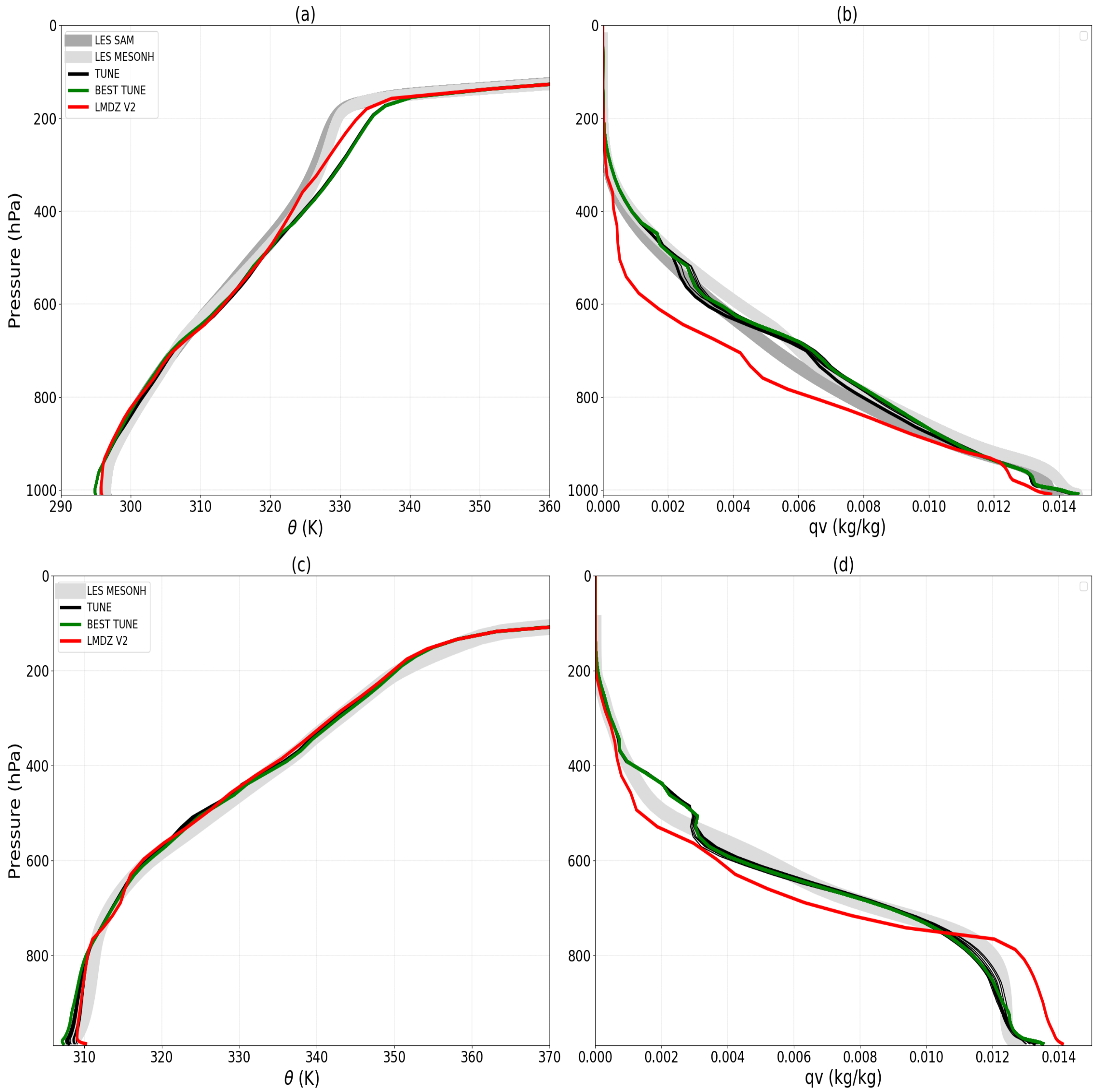

Figure 11: Like ~~Fig. ??~~Fig. 9, but ~~including~~ showing for LMDZ, the V2 simulation, the 12 best simulations from the tuning (TUNE, in black) as well as the best one among them (TUNE BEST, in green).

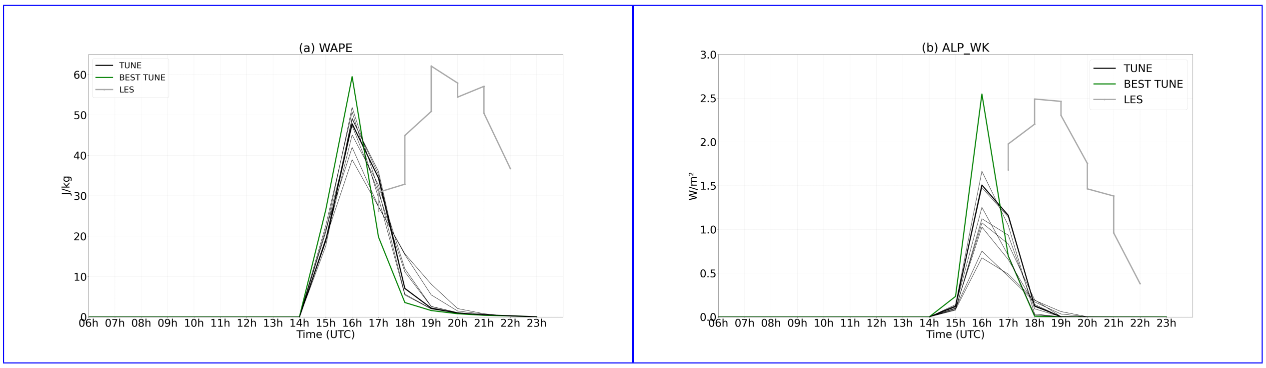

Figure 12: Time series of the collapse energy, $WAPE$ (J/kg, panel a), and the available lifting power,~~ALP_{wk}~~ ALP_{wk} (W/m^2, panel b), associated with cold pools, shown for the 12 best simulations from the tuning (TUNE, in black) and for the best among them (TUNE BEST, in green).

~~a sampling~~

For this, we introduce two samplings of the LES. The first one separates the interior from the outside of the cold pools~~in the LES~~, based on a threshold of the 10 m temperature anomaly of -0.2 K for the RCE case and -1 K for AMMA. The second one separates the zone of gust fronts by smoothing horizontally the vertical wind at cloud base (moving averaged over a square of 1.25 km side for the RCE case and 2 km for AMMA) with a threshold of 0.8 m/s for the CRE case and 2 m/s for AMMA. The coincidence of the temperature contour used for the cold pool sampling with the lines of maximum wind converge near the surface and with the gust front mask provides a very consistent view of the cold pools. It reinforces the choices that guided the conception of the cold pool scheme. It also confirms that most of the thermals reaching cloud base are located outside cold pools.

We started by validating relationship internal to the parameterizations, by diagnostics of the LES. The results show that the ~~ALE_{wk}~~ ALE_{wk} calculated from the $WAPE$ (computed from the vertical profile of the temperature anomaly between the cold pool and its environment) is comparable to that estimated from the vertical velocity in gust fronts w_{bgust}. This result is consistent with the model hypothesis, which estimates an equality between ~~ALE_{wk}~~ ALE_{wk} and $WAPE$. The spreading speed C_*, determined from the mean of divergence of wind at 10 m inside cold pools, is consistent with the estimate based on the square root of $WAPE$, if coefficient k entering in equation ((4)) is fixed to ~~0.66. This~~ 0.56, a value is consistent with ~~the work of Lafore and Moncrieff (1998), and differs from the initially assumed value of 0.33 in the model. ALP_{wk}~~ published values [Mettre les citations. Lamine : toutes les citations doivent être dans des cite Lafore and Moncrieff (1998)]. ALP_{wk}, calculated using C_* (computed from the $WAPE$ with ~~$k = 0.66$~~ $k = 0.56$), is close to the estimate derived directly from w_{bgust}. This result is compatible with the model hypothesis according to which a quarter of the cold pool Avaliable Potential Power, ~~ALP_{wk}~~ ALP_{wk}, feed deep convection, the remaining being dissipated. All of these results show the overall consistency of the model hypotheses with the three LES (RCE and AMMA) used in this study.

We then compare LES ~~simulations~~ results with the SCM version of LMDZ~~for the RCE and AMMA cases~~.

The results show that the initial version of the parameterization represents the cold pool properties well to first order, but with a dry anomaly in the cold pool region much too strong for the RCE case above the cold pool top, and a general tendency for both cases to underestimate the cold anomaly within cold pools and in turns $WAPE$, C_*, ~~ALE_{wk} and ALE_{wk}~~ALE_{wk} and ALE_{wk}.

The dry bias simulated at the top of cold pools is attributed to the ~~maximum subsidence altitude (h_m~~pressure of the maximum subsidence height (p_{upper}) which was imposed at a fixed value of 600 hPa in the original scheme. This value which was inspired from continental situations is well suited for the AMMA case but much to small for the RCE case for which the LES indicate a value of about 800 hPa. Making ~~h_m dependent on h_{wk}~~p_{upper} dependent on p_{wk}, the pressure at cold pool top, we significantly improve the simulated humidity at the top of cold pools for both cases. These results highlight the ~~significant impact of descending air masses in cold pools on the vertical~~ control of the cold pool humidity anomaly profile by lateral entrainment of dry air from the mid troposphere and subsidence within the cold pool. They also confirm the relevance of the cold pool transport model with lateral entrainment between ~~h_m and h_{wk}~~ p_{upper} and p_{wk} feeding the maximum subsidence at ~~h_{wk}~~p_{wk}.

Increasing the value of coefficient k from 0.33 to ~~0.66~~0.56, as suggested by the analysis of the LES, almost doubles the estimation of C_* for both the RCE and AMMA cases and multiplies the value of ~~ALP_{wk}~~ ALP_{wk} by 6 for AMMA and more than 10 for the RCE case, without affecting much the vertical mean and anomaly profiles. However, despite this improvements, C_* and ~~ALP_{wk}~~ ALP_{wk} remain underestimated in both cases.

A wet bias is also obtained at the surface of cold pools in the RCE and AMMA cases. Our analyses show that this bias is linked to the absence, in the model, of the effect of thermals on the variation of humidity at the surface of cold pools. The evaporation flux plays a weak role in this variation, which seems to be mainly controlled by thermals. ~~To account for the effect of thermals on humidity variation in cold pools, we propose to introduce a parameterization of shallow thermals (not producing clouds) inside cold pools.~~

Despite all the improvements, the cold pools remain not cool enough in the RCE case, inducing an underestimation of C_* by about 25% and ~~ALP_{wk}~~ ALP_{wk} by a factor of 3. In the AMMA case, where the cold pools are colder, the value of C_* is, conversely, overestimated by about 35%, while that of ~~ALP_{wk}~~ ALP_{wk} remains underestimated by a factor of 4. In order to check whether this limitation may come from a coupling with the other model parameterizations, and in particular that of deep convection, we conducted a calibration experiment using the HighTune explorer software to jointly adjust the free parameters of the cold pools and deep convection models. This tuning procedure also aimed to correct the dry and wet biases still present in the potential temperature and specific humidity profiles.

These adjustments led to a significant improvement in the representation of cold pool temperature, as well as specific humidity for the RCE and AMMA cases, even if a humid and cold bias persists in the boundary layer for the AMMA case. The values of $WAPE$, ~~ALP_{wk}~~ ALP_{wk} and C_* are also improved.

The above mentioned changes have been adopted in the new version of the LMDZ global model, used as the atmospheric component of the IPSL-CM7 coupled model under development for the forthcoming CMIP7 Fast-Trac exercise.

Although significant progress has been made in recent years in modeling cold pools, due to their important role in convection, challenges remain. First a simple parameterization of boundary layer convective transport, based for instance on a simplified version of the thermal plume model, could be included to better represent vertical mixing within the cold pools without activating the thermal plume model uniformly over the grid cell. The cold pool number density should become an internal variable of the model since we know it presents very different values when considering popcorn like convection over ocean or continents, or well organized long live system such as squall lines. A parameterization of this number density, based on a population dynamic model is presently under test. To end with, the issue of the propagation of cold pools from grid cell to grid cell needs to be also integrated into GCMs.

A ~~Tungin experiment~~ and the tuning setup

A.1 High-Tune Explorer (~~HTExplo~~htexplo) tool

~~General circulation models, used for global warming projections, are essentially based on a separation between the dynamical core, which manages large-scale air movements, and the physical parameterizations, enabling the impact of subgrid processes on the large scale to be represented. Progress in improving these models has been slow in recent years, not only because of the difficulties of integrating these processes into the parameterizations, but also because of the complex tuning of the many free parameters involved in their formulation. This is the background to the development of the High-Tune Explorer (HTExplo)~~

The tuning experiments shown here are done with the `htexplo` tool.

~~HTExplo~~ `htexplo` has been developed in collaboration between the LMD (Paris), the Centre National de Recherche Météorologiques (CNRM/Météo-France) and the University of Exeter (UK). It is an automatic calibration tool for free parameters, based on machine learning techniques from the uncertainty quantification community (?). This approach proposes a new calibration paradigm: instead of optimizing parameter values, it aims to identify the subset of parameters that enables the model to reproduce certain observables to a certain accuracy. The main steps involved in using the tool, as well as its mathematical foundations, are well described in ?. The ~~HTExplo~~ `htexplo` tool was used for the first time in a SCM/LES comparison on several boundary layer cases of the LMDZ model, in order to characterize the subspace of free parameter values for which SCM simulations are consistent with LES for certain metrics and a given tolerance (?). This information was then used by ? to calibrate the 3D configuration. These authors demonstrated how

metric	unit	target	tolerance
RCE case, average from day 41 to day 43			
WAPE	$m^2\ s^{-2}$	8	2
C_*	$m\ s^{-1}$	2.2	0.2
$\delta\theta_{0\text{-}50\ m}$	K	-0.83	0.045
$\delta\theta_{0\text{-}600\ m}$	K	-0.48	0.063
$qv_{0\text{-}500\ m}$	g/kg	14.1	0.45
$qv_{1\text{-}3\ km}$	g/kg	9.14	0.45
$qv_{5\text{-}6\ km}$	g/kg	2.55	0.33
$qv_{8\text{-}10\ km}$	g/kg	0.289	0.063
$\theta_{0\text{-}500\ m}$	K	296.5	1.47
$\theta_{1\text{-}3\ km}$	K	301.0	1.
$\theta_{5\text{-}6\ km}$	K	317.4	1.
$\theta_{8\text{-}10\ km}$	K	328.8	3.
AMMA case, average from 10:00 AM to 5:00 PM			
WAPE	$m^2\ s^{-2}$	20	3

Table 6: Metrics (targets and 1-σ tolerances) used for the tuning. For the RCE case, they concern the averages between days 41 and 43 of the WAPE and the cold pool spreading rate C_*, as well as the vertical profiles of $\delta\theta$, qv, and θ averaged over the altitude ranges specified in the right column. For the AMMA case, only the WAPE averaged between hours 10 and 17 of the simulation is used.

Parameter	units	[min,max] prior	exploration	[min , max] 12 best simulations
Cold pool model				
ϵ (équation 18)	-	[0.25 , 0.5]	linear	[0.26 , 0.46]
$\gamma_{\text{wk,upper}}$	-	[3.5 , 5]	linear	[3.6 , 4.1]
k (équation 4)	-	[0.33 , 0.66]	linear	[0.56 , 0.57]
σ_{int}	-	[0.75 , 0.99]	linear	[0.96 , 0.987]
Convection model				
wb_{srf}	m/s	[0.5 , 1.2]	linear	[0.55 , 0.98]
wb_{max}	m/s	[2.8 , 6]	linear	[2.8 , 3.5]
$\sigma_{\text{desc.}}$	-	[0.015 , 0.05]	linear	[0.042 , 0.048]
1-EP_{max}	-	[0.05 , 0.1]	log	[.93 , .95]
$k_{\text{ALP,BL}}$	-	[0.2 , 0.5]	linear	[0.33 , 0.47]

Table 7: Free parameters considered in the tuning exercise.

reducing the parameter space using this method significantly saves computing and human resources. They also pointed out that this approach eases the burden on the modeler, enabling him or her to concentrate more on understanding and improving the physical parameterizations of the model.

For the RCE case, we target the quasi-equilibrium phase by considering averages between days 41 and 43. The metrics selected for these calibration exercises are the profiles of δT, q_v, and θ, evaluated from vertical averages at different levels as indicated in.

Details on the metrics, with targets and tolerances to error, are given in Table 6.

The parameters chosen for tuning are listed in Table 7 together with the a priori ranges given to `htexplo` at the beginning of the tuning exercise and ranges of the best 12 simulations obtained after 13 waves of tuning.